Journal of Medicinal Chemistry

Article

Discovery, Optimization and Evaluation of Potent and Highly Selective PI3K#-PI3K# Dual Inhibitors

Hong Jia, Guangxiu Dai, Weiguo Su, Kun Xiao, Jianyang Weng, Zhulin Zhang, Qing Wang, Tianhai Yuan, Fuying Shi, Zheng Zhang, Wei Chen, Yang Sai, Jian Wang, Xiong Li, Yu Cai, Jun Yu, Ping Ren, Jennifer Venable, Tadimeti Rao, James Patrick Edwards, and Scott D. Bembenek

J. Med. Chem., **Just Accepted Manuscript** • DOI: 10.1021/acs.jmedchem.8b02014 • Publication Date (Web): 29 Apr 2019

Just Accepted

ACS Publications

is published by the American Chemical Society. 1155 Sixteenth Street N.W., Washington, DC 20036

Discovery, Optimization and Evaluation of Potent and Highly Selective PI3Kγ−PI3Kδ Dual Inhibitors

Hong Jia[‡], *Guangxiu Dai*[‡]*, *Weiguo Su*[‡], *Kun Xiao*[‡], *Jianyang Weng*[‡], *Zhulin Zhang*[‡], *Qing Wang*[‡], *Tianhai Yuan*[‡], *Fuying Shi*[‡], *Zheng Zhang*[‡], *Wei Chen*[‡], *Yang Sai*[‡], *Jian Wang*[‡], *Xiong Li*[‡], *Yu Cai*[‡], *Jun Yu*[‡], *Ping Ren*[‡], *Jennifer Venable*[#], *Tadimeti Rao*[#], *James P. Edwards*[##], *Scott D. Bembenek*[#].

[‡]Hutchison MediPharma Limited, Building 4, 720 Cai Lun Road, Zhangjiang Hi-Tech Park, Shanghai 201203, China;

[#]Janssen Pharmaceuticals Research & Development, 3210 Merryfield Row, San Diego, CA 92121, United States

[##]Janssen Pharmaceutical Research & Development, 1400 McKean Road, Spring House, PA 19477, United States

*Correspondence author: guangxiud@hmplglobal.com

KEYWORDS: PI3Kγ, PI3Kδ, Phosphoinositide 3-kinases, kinase inhibitors, structure-based drug design, SBDD, RA, rheumatoid arthritis.

ABSTRACT: An electronic density model was developed and used to identify a novel pyrrolotriazinone replacement for a quinazolinone, a commonly used moiety to impart selectivity in inhibitors for PI3Kγ and PI3Kδ. Guided by molecular docking, this new specificity piece was then linked to the hinge–binding region of the inhibitor using a novel cyclic moiety. Further SAR optimization around the hinge region led to the discovery of candidate **26,** a highly potent and selective PI3Kγ−PI3Kδ dual inhibitor with favorable DMPK properties in preclinical species.

INTRODUCTION

Phosphoinositide 3-kinases (PI3-kinases or PI3Ks) are a family of enzymes involved in cellular functions such as cell growth, proliferation, differentiation, motility, survival and intracellular trafficking. Based on the sequence homology and lipid substrate specificity, the PI3K family is divided into class I, class II, and class III. The class I PI3Ks are the most extensively studied and the focus of numerous drug discovery efforts. All class I PI3Ks are heterodimeric proteins. Each contains a small regulatory domain and a large 110 kDa catalytic domain which occur in four isoforms differentiated as p110α, p110β, p110γ and p110δ.[1-3]

All four class I catalytic PI3K isoforms show a characteristic expression pattern *in vivo*. PI3Kα and PI3Kβ are ubiquitously expressed and play key roles in cell growth, survival, and proliferation; inhibition of PI3Kα and PI3Kβ mainly targets cancer therapy.[4-5] PI3Kγ is widely expressed in granulocytes, monocytes, and macrophages, while the PI3Kδ isoform is also found in B and T cells. Mice containing knockouts for the genes encoding either PI3Kδ or PI3Kγ are viable and fertile but exhibit significant defects in innate immunity as well as adaptive responses.[6-8] Thus isoform-specific PI3Kδ or PI3Kγ inhibitors may have therapeutic benefits on autoimmune diseases without interfering with the general PI3K signaling critical to the normal functions of other cellular systems.

Rheumatoid arthritis (RA) is an immune-mediated disease causing debilitating joint inflammation and tissue damage. The activities of T cells, B cells, mast cells, macrophages, and neutrophils have all been shown to affect at least one or several aspects of the disease. Considering their functions in these cells, their activities and the abundant expression in RA synovium and fibroblast-like synoviocytes (FLSs), PI3Kγ and PI3Kδ represent possible therapeutic targets for rheumatoid arthritis.[6, 9-11]

Several PI3Kδ inhibitors have entered clinical development. Idelalisib, also known as GS-1101 or CAL-101 and branded Zydelig™, (**1** in **Figure 1**), is the first FDA-approved PI3Kδ inhibitor to treat follicular lymphoma (FL), and small lymphocytic lymphoma (SLL) as a single agent, and to treat relapsed chronic lymphocytic leukemia (CLL) in combination with anti-CD20 Rituximab.[12] Umbralisib (TGR-1202) (**2** in **Figure 1**) is a small molecule PI3Kδ inhibitor developed by TG Therapeutics and is currently in Phase 3 clinical trials in combination with anti-CD20 ublituximab (TG-1101) for patients with hematologic malignancies.[13] In recent years, more selective PI3Kδ inhibitors have been advanced into clinical trials.[14]

Discovery of PI3Kγ specific inhibitors have faced the challenge of isoform selectivity due to high homology between PI3Kγ and PI3Kα. Infinity Pharmaceuticals reported a highly potent and selective PI3Kγ inhibitor IPI-549 (**3** in **Figure 1**), which is being evaluated in a Phase 1 study as a monotherapy and in combination with nivolumab in patients with advanced solid tumors.[15]

Although inhibition of either PI3Kγ or PI3Kδ alone presents a unique therapeutic opportunity in autoimmune and oncology diseases, simultaneous inhibition of both these isoforms may yield superior clinical efficacy in the treatment of a variety of complex immune-mediated inflammatory diseases.[16-17] Both enzymes are known to help support the growth and

survival of malignant B-cells and T-cells. They play a role in the formation and maintenance of the supportive tumor microenvironment.Targeting both PI3Kγ and PI3Kδ for oncology indications, such as chronic lymphocytic leukemia, acute myeloid leukemia, non-Hodgkin's lymphoma, multiple myeloma also has been studied.[18-19]

Duvelisib (**4** in **Figure 1**, IPI-145) and branded COPIKTRA™, the first reported dual inhibitor of PI3Kγ and PI3Kδ by Infinity Pharmaceuticals, demonstrated that the combined inhibition of adaptive and innate immune function can be achieved through dual blockade, leading to significant therapeutic advantage in multiple inflammatory and autoimmune diseases in animal models.[20] However, duvelisib failed to demonstrate a positive clinical response in RA patients in a double-blind, placebo-controlled Phase 2 study with background methotrexate.[21] Based on our own PKPD modeling, we speculated that neither clinical dose (1 mg and 5 mg, both twice daily) would provide sufficient drug exposure to suppress both targets, (especially PI3Kγ), to produce a clinical response. In 2018, duvelisib was approved for the treatment of patients with relapsed or refractory chronic lymphocytic leukemia/small lymphocytic lymphoma and follicular lymphoma. Rhizen Pharmaceuticals S.A. have also completed a Phase 1 clinical study with the PI3Kγ−PI3Kδ dual inhibitor tenalisib (RP-6530) (**5** in **Figure 1**) to treat patients with relapsed or refractory hematologic malignancies, including T-cell Lymphoma. [22-23]

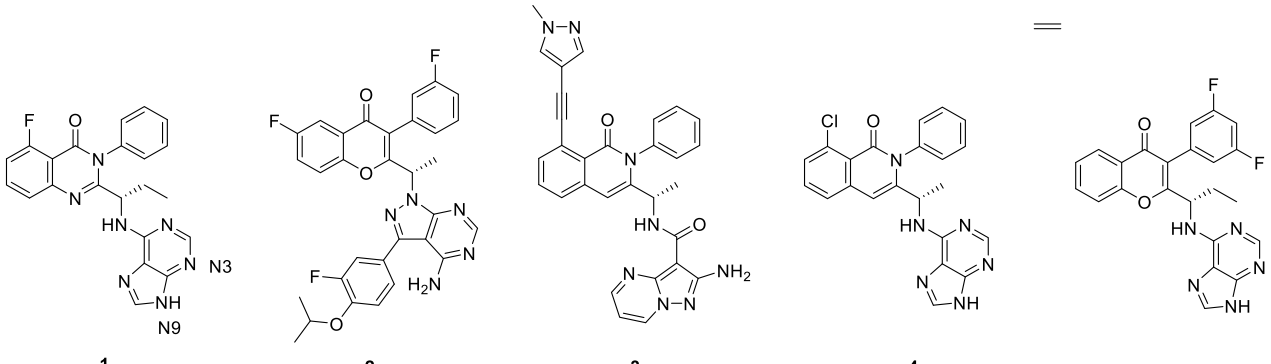

Figure 1. Structures of PI3Kδ and PI3Kγ inhibitors

Here, we describe our efforts toward identifying a novel series of potent and highly selective PI3Kγ–PI3Kδ dual inhibitors, which led to the discovery of the efficacious and orally bioavailable **26** as a drug candidate for treating RA and other autoimmune diseases.

RESULTS AND DISCUSSIONS

Molecular docking was used to identify the key interactions of **1** in the ATP binding pocket of both PI3Kγ and PI3Kδ. **Figure 2** show these interactions for **1** docked in PI3Kγ. Here we see N3 and N9 of the purine hinge-binding region of the molecule form hydrogen bonds with the backbones residues V882 and E880 respectively (In PI3Kδ, the corresponding residues are V828 and E826). The quinazolinone motif, or specificity piece, makes a hydrophobic interaction with M804 (M752 in PI3Kδ) and an edge-on-π interaction with W812 (W760 in PI3Kδ). The interaction with W812 is hypothesized to be the stronger of the two interactions, as it is a specific interaction involving the proximal proton of W812 directly interacting with the π system of the quinazolinone (seen in **Figure 2**). We note that this proposed docking mode was in excellent agreement with the later reported X-ray crystal structure of **1** bound in the PI3Kδ (4XE0 in PDB) [12]. Moreover, based on our modeling and known literature crystal structures, compounds **2**, **4** and **5** are expected to have binding poses similar to **1** in both PI3Kγ and PI3Kδ.

The aforementioned interactions of **1** and overall low-strain fit into the binding pocket mostly ensure its potency in both PI3Kγ and PI3Kδ. [25] Further, ligands engaging the P-Loop with a specificity piece tend to have excellent overall kinome selectivity while showing a varying degree of activity over the PI3K isoforms.[13] Given the variations in conformational plasticity of the P-Loop (note that the similarity in the P-Loop among the PI3K isoforms ranges between 65–68%) and that distinction in its overall interaction with the specificity piece of a ligand exists, [24] we expected that this region could provide an opportunity to achieve PI3K isoform selectivity. [25]

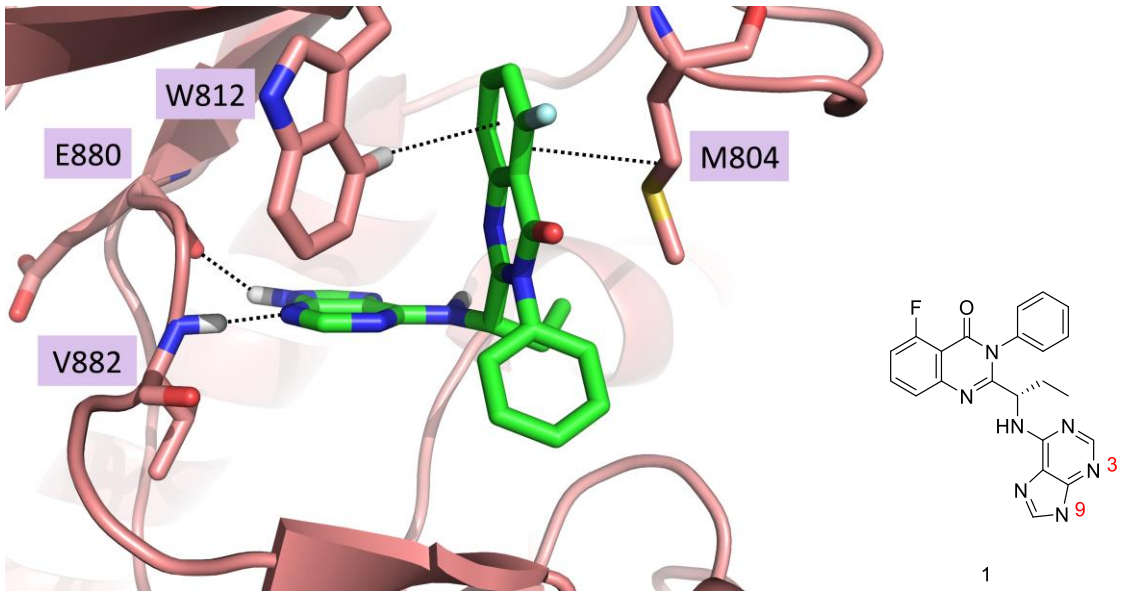

Figure 2. Proposed docking pose of **1** in PI3Kγ. The hinge region makes hydrogen bond interactions with the backbones of V882 and E880. The specificity piece (shown in the box), makes a hydrophobic interaction with M804, and an edge-on-π interaction with W812, which is the stronger of the two interactions. 2CHW in PDB was used for the modeling.

The first goal of the program was to identify a replacement for the quinazolinone in **1** that would present more favorable DMPK properties. Ideally this novel specificity piece would achieve both similar fit and interactions (especially with W812) in the P-Loop region.

As the first step in identifying viable replacement specificity piece motifs, a virtual screen was performed on that portion of the molecule using the bioisostere replacement tool BROOD.[26] We found the results from BROOD to be of more qualitative, rather than quantitative, value. In other words, while BROOD provides a viable means of lead hopping and brainstorming, we have found the actual score to be of little value in prioritizing molecules for synthesis.

Seeking a scoring tool that would be more useful for prioritization of medicinal chemistry efforts, motifs of interest from the BROOD virtual screen were subsequently run through the

electrostatic similarity tool EON, [27] whereby we obtained an electrostatic surface representation for each novel motif along with the original reference motif (quinazolinone) of **1**. We then hypothesized the major interaction of the specificity piece was on the side interacting with W812. Finally, through visual inspection of the electrostatic surfaces (**Figure 3)**, we sought out those new motifs that were comparable to **1** on that side. (In the supporting information, we showed examples of poor affinity specificity pieces and their electrostatic surfaces. **See Figures S1**–**S4**.) Although EON does provide an overall score for each piece against the chosen reference (e.g., **1**), we found it to be in poor agreement with our SAR. We therefore pursued the described visual inspection approach as a feasible alternative.

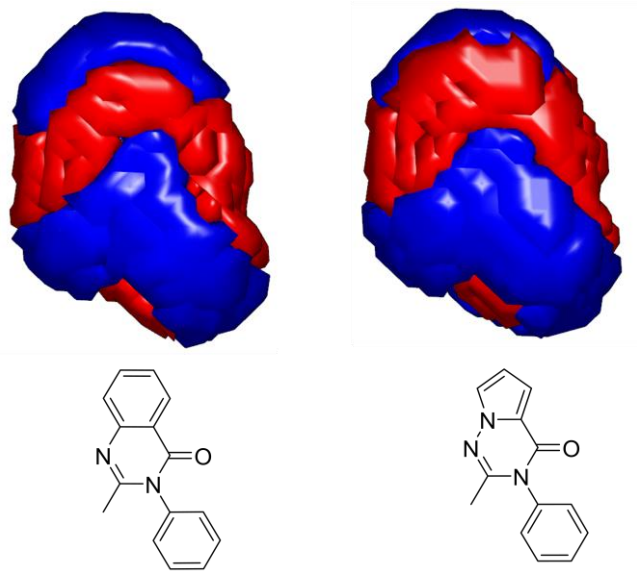

Figure 3. The electrostatic surfaces of the (parent) specificity pieces for compound **1** (quinazolinone) and the (electronically similar) novel pyrrolotriazinone motif identified from modeling.

In this way, several novel replacement motifs for the specificity piece were identified. However, it was the pyrrolotriazinone that showed the most electronic similarity (according to

the described paradigm) to the quinazolinone motif of **1**, and therefore was chosen for successive chemistry. We describe our lead optimization of the pyrrolotriazinone series of PI3Kδ/γ inhibitors in detail below.

The docking mode of **1** in PI3Kγ (**Figure 2**) showed the open-chain-amine linker placed the specificity piece and the hinge perpendicular to each other resulting in a propeller-like shape. Given the overall orientation of the molecule along with its interactions within the binding pocket, we realized that cyclization of the linker into a 5-membered pyrrolidine would be a feasible approach for structural modification to reinforce parameters by locking the conformation (**Figure 4**). This proposal was further substantiated upon docking of the *de novo* compound **6** (and subsequently **7**) in PI3Kγ, which displayed key interactions (in the hinge and specificity pieces regions) and overall fit in the binding pocket (**Figure 5)** to be comparable to **1**. The docking model also revealed that the new cyclic-amine linker would more fully occupy (than the open-chain-amine linker) a small hydrophobic pocket formed by M804, I963 and M953.

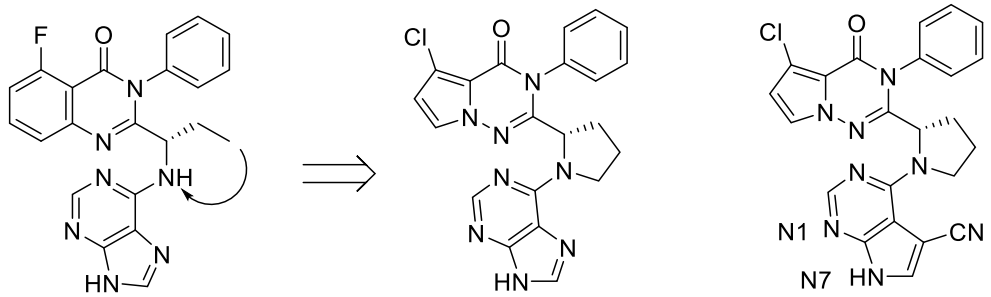

1 **6** **7**

Figure 4. Rational design of PI3Kγ and PI3Kδ inhibitors.

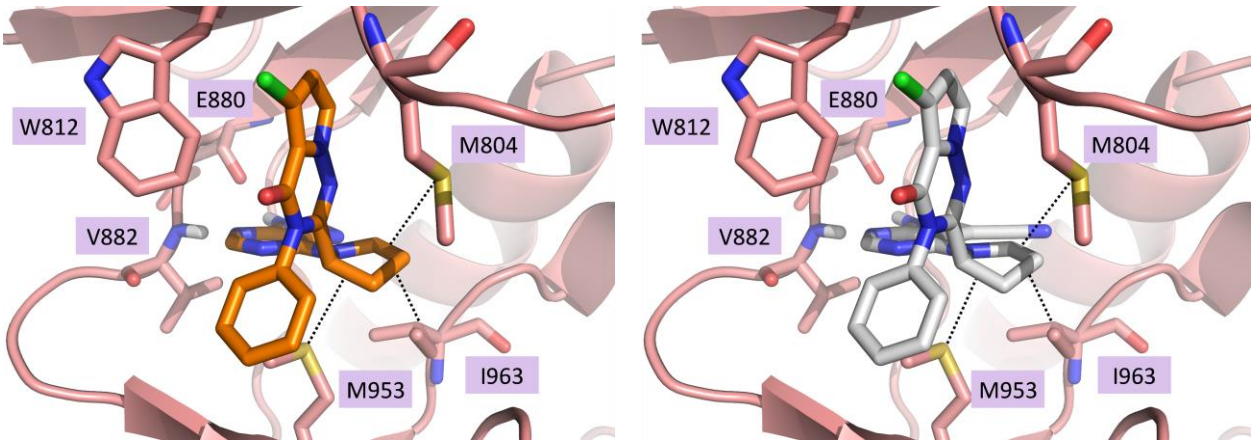

Figure 5. Docking models of **6** (left) and **7** (right) in PI3Kγ. Hydrophobic interactions occur within a small pocket formed by M804, I963 and M953. 2CHW in PDB was used for the modeling.

As predicted from the docking model, **6** showed good inhibition of both PI3Kγ and PI3Kδ with an IC_{50} of 0.012 μM and 0.002 μM, respectively. Compound **6** retained equivalent activity for PI3Kδ and improved activity for PI3Kγ compared to compound **1** (**1**: IC_{50} = 0.104 μM and 0.002 μM in PI3Kγ and PI3Kδ in biochemical assays). With an IC_{50} of 0.004 μM and 0.001 μM in PI3Kγ and PI3Kδ respectively, **7** demonstrates improved activity at PI3Kγ and is comparable to **4** (IC_{50} = 0.002 μM and 0.001 μM in PI3Kγ and PI3Kδ respectively)**.** These data helped verify the docking model as well as confirmed the success of replacing quinazolinone with pyrrolotriazinone and cyclic linker. However, both **6** and **7** both displayed poor metabolic stability in rat liver microsomes and further improvement in isoform selectivity over PI3Kβ was still needed. Initial SAR investigations were primarily focused on improving the selectivity profile of **6** and **7** while monitoring the impact on metabolic stability in rat and human liver microsome assays. Modifications were evaluated at key locations on the chemotype: C-5 of the pyrrolotriazinone (R_1), C-3 of the pyrrolidine (R_2), and the hinge-binding region of the molecule (W). As shown in **Table 1**, when C5-Cl of **6** was changed to F or H, the resulting analogs **8** and **9**

respectively demonstrated 5.6-fold and 9-fold lower activities against PI3Kγ. (In the supporting information, we compared the electrostatic surfaces of all three. See **Figures S5**–**S6**.). Introduction of a F in either the R_2 or R_3 positions (**10 and 11**) increased the isoform selectivity over PI3Kβ (IC_{50} ratio of PI3Kβ/γ is 26 for **10**; ~ 90 for **11**), while retaining potent IC_{50} values respectively (PI3Kγ: 0.016 μM, 0.011 μM; PI3Kδ: 0.003 μM). Removal of Cl at R_1 in **7** gave the unsubstituted compound **12**, which was 50-fold more selective over PI3Kβ comparatively with only a slight loss in potency against PI3Kγ, although significant instability in liver microsomal assays was noted. Finally, the *m*-F phenyl compound **13** displayed comparable on-target activities and isoform selectivity as **7**.

The (*R*)-enantiomers proved to be much less active. The (*R*)-enantiomer of **9** showed only 14.4% inhibition of PI3Kγ and 17.7% inhibition of PI3Kδ at 1 μM. Similarly the corresponding (*R*) isomer of **12** inhibited PI3Kγ and PI3Kδ by 21.2% and 7.7% at 1 μM, respectively. Changes to the hinge W were evaluated next. Altering the C-3 nitrile of the pyrimidinyl indole **7** to methyl ketone in compound **14** resulted in the improved selectivity of PI3Kγ and PI3Kδ over PI3Kβ by 3 fold with similar on-target activities as **7**. Combination of modifications to R_1 and R_2 with this new hinge resulted in compounds **15-17.** The addition of a F to the pendant phenyl or the pyrrolidine linker, and exchanging Cl with F, maintained equivalent potencies and similar selectivity. We also evaluated a 2-amino pyrimidine-5-carbonitrile hinge motif as in **18**. Potency and selectivity of this molecule was comparable to **14** (IC_{50} = 0.007 μM, 0.001 and 0.298 respectively for PI3Kγ, PI3Kδ and PI3Kβ). In terms of PI3Kα, all compounds showed less than 50% inhibition at 1 μM, except **4** (81%).

As in the enzymatic assays, compounds **10**-**12** and **16**-**18** were consistently potent in C5a-induced and anti-IgM induced phosphorylation of Akt kinase, with single-digit nanomolar $IC_{50's}$

in PI3Kδ and <0.050 μM in PI3Kγ. Unfortunately, these compounds displayed poor to moderate stabilities in either human or rat liver microsomes after incubation for 30 min (**Table 1**), and were predicted to be rapidly cleared in rodents.

Table 1. SAR of pyrrolidine-linker compounds.[a]

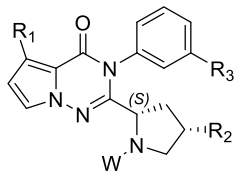

Cpd	R_1	R_2	R_3	W	PI3K enzyme IC_{50} (μM)[c]			PI3K cell IC_{50} (μM)		Microsomal stability, remaining (%)	
					γ	δ	β	γ	δ	RLM	HLM
1 (CAL-101)					0.104	0.002	0.293	0.337	0.004	--	--
4 (IPI-145)					0.002	0.001	0.008	0.025	0.001	--	--
6	Cl	H	H	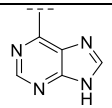	0.012	0.002	0.091	--	--	38.8	72.6
7	Cl	H	H	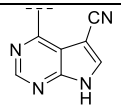	0.004	0.001	0.034	--	--	38.7	--
8	F	H	H	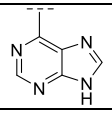	0.067	0.003	52.9%[b]	--	--	51.8	--
9	H	H	H	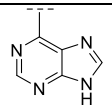	0.108	0.010	17.4%[b]	--	--	44.3	--
10	Cl	F	H	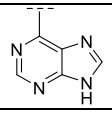	0.016	0.003	0.420	0.020	0.001	43.8	--
11	Cl	H	F	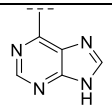	0.011	0.003	54.8%[b]	0.008	0.003	34.6	64.3

12	H	H	H	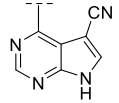	0.019	0.002	47.7% [b]	0.040	0.003	19.1	2.8
13	Cl	F	H	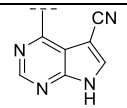	0.003	0.001	0.025	--	--	--	--
14	Cl	H	H	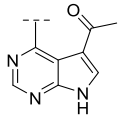	0.002	0.0005	0.051	--	--	41.4	17.9
15	Cl	F	H	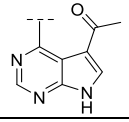	0.013	0.003	0.170	--	--	60.4	20.1
16	Cl	H	F	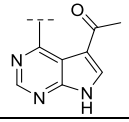	0.006	0.002	0.191	0.007	0.003	--	11.7
17	F	H	H	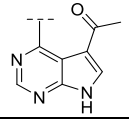	0.004	0.002	0.165	0.042	0.005	26.1	25.1
18	Cl	H	H	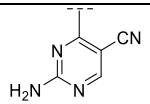	0.007	0.001	0.298	0.022	0.003	23.5	--

--: Not tested; [a]: IC_{50} or percentage of inhibition is based on a single run of experiments except **4** (n=3); [b]: Percentage of inhibition at 1 μM; [c]: all compounds showed less than 50% inhibition at 1 μM, except **4** (81%), in the PI3Kα enzymatic assay.

Further PK & metabolite ID studies showed that the oxidation of the pyrrolidine linker was one of the major metabolism pathways of these compounds (**Figure 6**). To increase the metabolic stability by mitigating the oxidation of the hydrophobic pyrrolidine, a 4-membered ring azetidine linker was introduced, which reduced clogP and maintained the propeller conformation essential for potency and selectivity. As expected, the metabolic stability of the azetidine compounds was improved compared to the corresponding pyrrolidine compounds. For example, percent remaining of the azetidines **20**, **21**, and **22** in rat microsomes was 63.9%, 77.2% and 77.5% respectively, and is much improved when compared to the corresponding pyrrolidine analogs **7**, **14** and **18**. This trend towards increased stability is also evident in the human liver microsomes (**Table 2**).

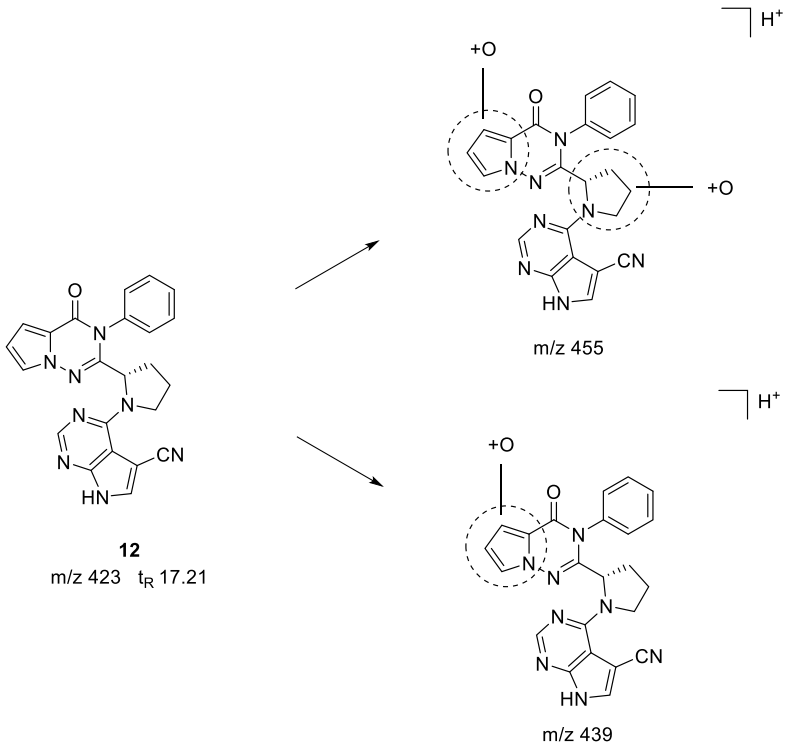

Figure 6. *In vitro* metabolite identification of **12** in human and mouse liver microsomes.

Surprisingly, while stability was improved in the azetidine analogues, both enzymatic and cellular activities decreased significantly. The enzymatic inhibition of **19** was much weaker against PI3Kγ and PI3Kδ (IC_{50} = 0.271 μM and 0.084 μM respectively) than the corresponding pyrrolidine **6**. Improved selectivity over PI3Kβ was seen for **20** when compared to **7** (PI3Kβ/γ = 28, PI3Kβ/δ= 73), but 8-fold less potent at PI3Kγ and 13-fold weaker at PI3Kδ with an IC_{50} of 0.034 μM and 0.013 μM respectively. Also, the inhibition of Akt phosphorylation was significantly impacted (IC_{50} = 0.152 μM and 0.021 μM, respectively). Consistent with the pyrrolidine analogue **14**, **21** was still active in the enzymatic assays (IC_{50} = 0.005 μM for PI3Kγ and 0.006 μM for PI3Kδ), and it showed much improved selectivity over PI3Kβ (~ 200 fold). Although **21** was still active and selective in the enzymatic assays, it exhibited reduced potency in C5a-induced phosphorylation of Akt with an IC_{50} of 0.142 μM. While the 2-aminopyrimidine hinge binding motif in **22** displayed diminished activity, it was still potent at PI3Kγ (IC_{50} = 0.027 μM) and PI3Kδ (IC_{50} = 0.012 μM) and selective (37.0% inhibition against PI3Kβ and < 50% against PI3Kα at 1 μM in enzymatic assay) (**Table 2**).

Table 2. SAR of azetidine-linker compounds [a]

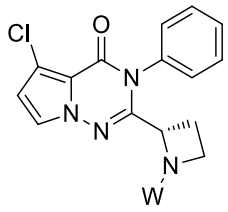

Cpd	W	PI3K enzyme IC_{50} (μM)				PI3K cell IC_{50} (μM)		Stability (%)	
		γ	δ	β	α	γ	δ	RLM	HLM
19	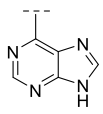	0.271	0.084	18.5% [b]	-1.5% [b]	--	--	78.5	95.4
20	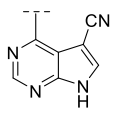	0.034 ± 0.009 (n=3)	0.013 ± 0.001 (n=2)	0.945	-0.3% [b]	0.152 ±0.090 (n=5)	0.021 ±0.001 (n=2)	63.9	89.8

21	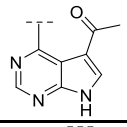	0.005	0.006	45.9% [b]	8.4% [b]	0.142 ±0.056 (n=2)	0.021 ±0.013 (n=2)	77.2	83
22	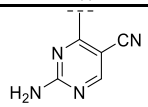	0.027	0.012	37.0% [b]	<50% [b]	0.241	0.016	77.5	71.2

--: Not tested; [a.] IC_{50} or percentage of inhibition is based on a single run of experiments; [b]: Percentage of inhibition at 1 μM

The balanced profile of compound **22** along with the ability to readily modulate the C-5 substituent led us to explore the SAR of the 2-aminopyrimidine as an effective hinge motif. As shown in **Table 3**, **23** demonstrated reduced biochemical potency than **22** towards PI3Kγ and PI3Kδ with an IC_{50} of 0.182 μM and 0.059 μM, respectively. Replacing the nitrile of compound **22** with an alkyne, resulted in **24,** which maintained isoform PI3K activities and selectivity in both enzymatic and cellular assays; however, the rat liver microsomal stability was only 8.9%. Changing nitrile of compound **22** to a methyl sulfone gave **25,** which had a complete loss of activities. The introduction of a methyl ketone into the C-5 position of the pyrimidine yielded **26,** which was both active and selective at PI3Kγ and PI3Kδ (IC_{50} at PI3Kα = 3.7 μM in enzyme and >10 μM in cell), as well as very potent on the inhibition of C5a and anti-IgM induced Akt phosphorylation (IC_{50} = 0.011 ±0.005 μM for PI3Kγ and 0.025 ±0.009 μM for PI3Kδ). *In vitro* ADME screening demonstrated that **26** was more stable in RLM and HLM (63.5% and 81.5%). Further modification of **26** to give the cyclopropyl (**27)** and CF_3 (**28)** did not produce the desired potency, indicating larger substitutes may not be well tolerated in this region.

Table 3. SAR of pyrimidine-hinge compounds.[a]

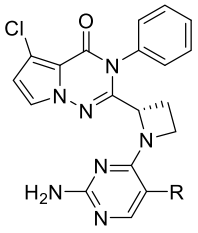

Cpd	R	PI3K enzyme IC_{50} (μM)		
		γ	δ	β
23	Cl	0.182	0.059	22.9% [b]
24		0.052	0.060	22.7% [b]
25		20.4% [b]	18.1% [b]	--
26		0.004 ±0.002	0.005 ±0.003	0.590 ±0.254
27		50.7% [b]	7.1% [b]	--
28		0.043	0.524	>1

--: Not tested; [a]: IC_{50} and percentage of inhibition is based on a single run of experiments except **26** (n=3); [b]: percentage of inhibition at 1 μM.

Compound **26** demonstrated high specificity towards the PI3K family in a panel of 458 kinases (395 non-mutated kinases and 63 mutated human kinases) at a test concentration of 10 μM. Furthermore, **26** showed nearly no activity against a panel of 50 GPCRs, ion channels, and transporters.

We further selected **26** for additional *in vitro* cellular assays to understand the impact on the functional activities of PI3Kδ and PI3Kγ. Assays for PI3Kδ functions include anti-IgM stimulated CD69 expression on B cells in human whole blood; anti-IgD stimulated CD86 expression on B cells in rat whole blood; and fMLP induced CD63 expression on basophils in human whole blood. Functional assays to evaluate PI3Kγ activity include anti-IgE induced CD63

expression on basophils in human whole blood. As shown in **Table 4**, **26** exhibited potent inhibitory effects on basophil and B cell activation. For example, IC_{50} was 0.042 μM and 0.337 μM on the inhibition of basophil activation in the human whole blood, and 0.044 μM on B cell activation in the rat whole blood.

Table 4. Additional cellular assays of compound **26** ($n \geq 3$)

Cpd	HWB B cell CD69 IC_{50} (μM)	RWB B cell CD86 IC_{50} (μM)	HWB basophil CD63 IC_{50} (μM)	
			Anti-IgE	fLMP
4	0.014±0.006	0.002±0.001	0.015±0.012	2.206±0.335
26	0.063±0.037	0.044±0.015	0.042±0.022	0.337±0.089

Experiments were performed in female Wistar rats to further evaluate the inhibitory effect of **26** on anti-IgD induced B cell activation e*x vivo*. Oral administration of **26** effectively inhibited anti-IgD induced B cell activation at 2h, with an inhibition of 88.3% at a dose of 1 mg/kg. Instillation of KC/GRO (also called CXCL1, Gro-α and neutrophil-activating protein 3 (NAP-3) ect, a CXC chemokine) into the rat subcutaneous air pouch induced robust neutrophil chemotaxis and this response is known to involve PI3K signaling[7]. In an air pouch study in rats, **26** blocked KC/GRO induced neutrophil migration at 4 h, with an inhibition of 87.9% at a dose of 10 mg/kg, confirming the potent inhibitory activity of **26** on PI3Kγ *in vivo.*

When administered *in vivo* for pharmacokinetic profiling, **26** demonstrated moderate clearance in rats and low clearance in dogs, moderate volumes of distribution, and high oral bioavailability (**Table 5**). No glutathione (GSH) adducts were identified in human liver microsomes when GSH was co- incubated as a cofactor.

Table 5. PK profiles of compound **26** in SD rats and in Beagle dogs.

Species	PO				IV				
	Dose (mg/kg)	F (%)	C_{max} (ng/mL)	AUC (h·ng/mL)	Dose (mg/kg)	Cl (mL/min/kg)	$T_{1/2}$ (h)	V_{ss} (L/kg)	AUC (h·ng/mL)
Rat[a]	10	107.9	2730	14342	2.5	12.7	1.5	1.2	3274
Dog[b]	5	82.4	2532	13125	1	5.4	6.3	1.7	3261

[a]: 20% HP-beta-CD, pH2.5; [b]: 20% HP-beta-CD, pH4.3. Values were the mean values of male for rats, male and female for dogs.

We dosed **26** in an established rat collagen-induced arthritis model at 0.1, 1 and 10 mg/kg twice daily for 7 days from day 10-16. It significantly reduced the average paw volumes in a dose-dependent manner, indicating significant anti-inflammatory effects; the estimated ED_{50} was 0.25 mg/kg, BID (**Figure 7**). Given at 1.0 mg/kg BID, **26** produced a paw volume reduction comparable to the positive control YiSaiPu (a rhTNFR: Fc) from day 11 to day 16; and a 10 mg/kg BID administration of **26** demonstrated strong efficacy from day 11 and reversed the disease progression nearly returning the animal back to normal on day 16.

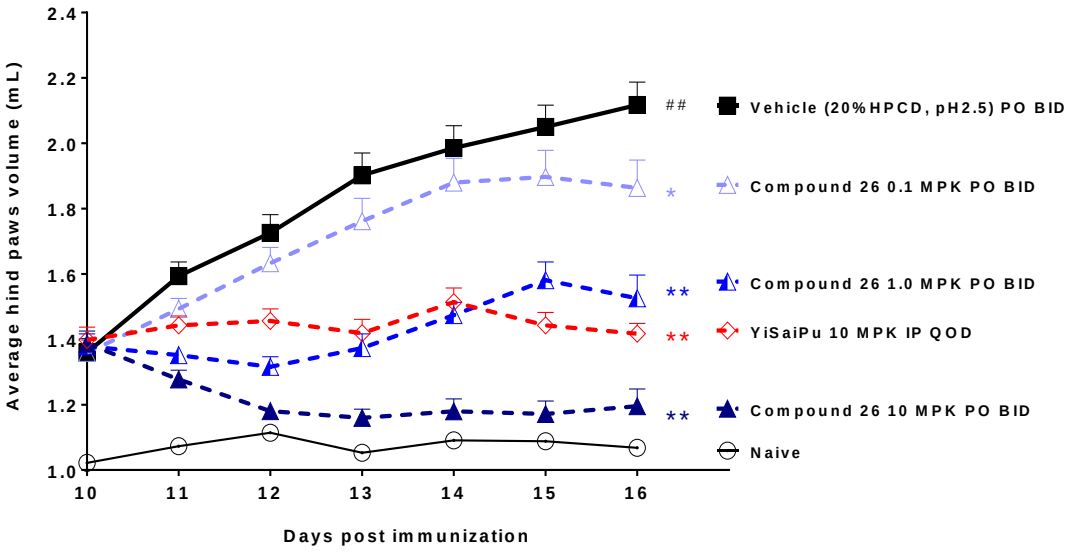

Figure 7. Hind paw swelling reduction of compound 26 in rat CIA model. The paw volume was expressed as mean ± SEM. n= 6 in Naive groups. n=9 in the other groups. *p<0.05, **p<0.01 vs vehicle group, #p<0.05, ##p<0.01 vs naive group. **26** was dosed twice daily for 7 days.

CHEMISTRY

Compounds **30a-e** were prepared starting with a coupling reaction between amide **29a-c** and various substituted proline or azetidine carboxylic acids, followed by intramolecular dehydration to produce **31a-e**.[28] The desired compounds were generated by two routes, depending on the nature of the R_2 substituent. When R_2 is not a hydroxyl, **31a-b** and **31d-e** were converted to **32a-e**.[29] After NBoc de-protection , **32a-e** were treated with the halides of the selected hinge motif W in SnAr reactions to give the final compounds **6-9**, **11-12, 14, 16-24** and **26**, as well as **25a** and **36a-b** as intermediates. If R_2 is hydroxyl, the compound was treated with DAST to introduce fluorine onto the pyrrolidine. The resulting compound **33** was used to make compounds **10, 13,** and **15** in a similar fashion as **6** (**Scheme 1**).

When W is 4-(2-amino-5-bromo)pyrimidinyl, **25a** was coupled with sodium methanesulfinate to give **25**. **36a-b** could be converted to compounds **27-28** by oxidation, followed by the displacement of sulfonyl with NH_2 (**Scheme 2**).

Scheme 1. Synthesis of compounds **6-26** and **i**ntermediates **25a, 36a-b** [a]

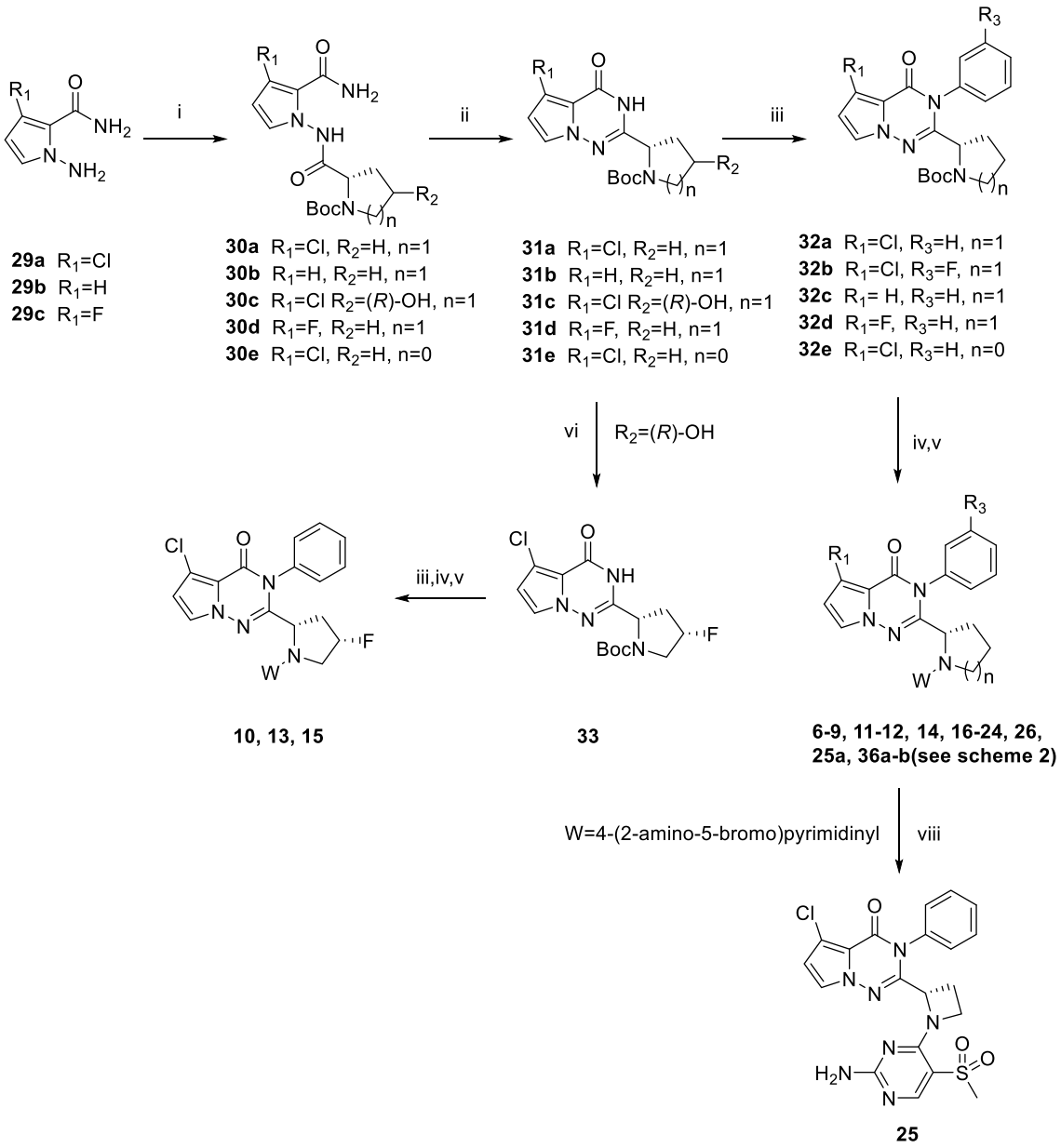

Reagents and conditions: (i) EDC·HCl, THF, rt; (ii) KOH, EtOH, H_2O, 100 °C; (iii) substituted or unsubstituted phenylboronic acid, 4Å molecular sieves, $Cu(OAc)_2$, pyridine, DCM, rt; (iv) aq. HCl or conc. HCl, MeOH; (v) *n*-BuOH, Et_3N, reflux; (vi) DAST, DCM, 0 °C to rt; (viii) sodium methanesulfinate, $Pd_2(dba)_3$, Xantphos, K_3PO_4, 120°C, N_2.

Scheme 2. Synthesis of compounds **27-28** [a]

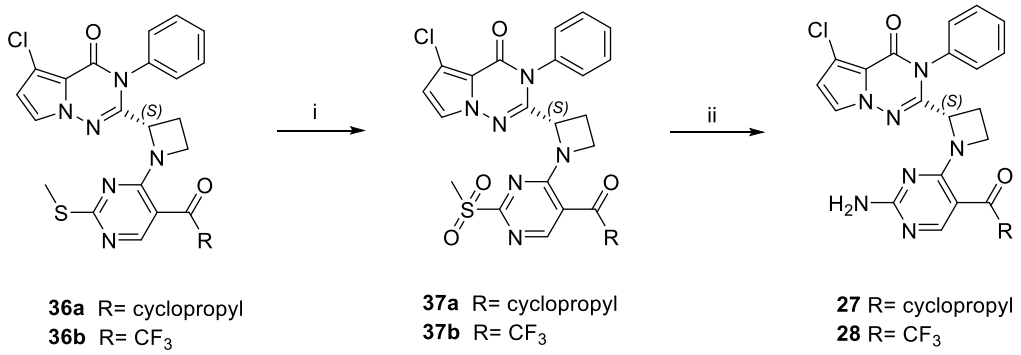

Reagents and conditions: (i) *m*-CPBA, DCM, 0 ^{o}C to rt.; (ii) DCM, NH_3, rt.

CONCLUSION

In conclusion a combination of an electronic density model approach and molecular docking led to design of a novel series of potent and isoform-selective PI3Kγ – PI3Kδ dual inhibitors characterized by a substituted pyrrolotriazinone specificity piece connected to the hinge-binding region of the molecule through a cyclic linker. After optimization of the hinge and linker, the azetidine **26** was identified as a promising preclinical candidate of PI3Kγ and PI3Kδ inhibitors with potent efficacy in a rat CIA model and desirable pharmacokinetic properties.

EXPERIMENTAL SECTION

All reagents and solvents employed were purchased commercially and used without further purification. Temperature and pressure is at or near atmospheric. NMR data were recorded on a Varian 400-MR machine. Chemical shifts are expressed as δ units using tetramethylsilane as the external standard (in NMR description, s, singlet; d, doublet; t, triplet; q, quartet; m, multiplet; and br, broad peak). All coupling constants (*J*) are reported in Hertz. MS data were checked by Agilent 6120 or Agilent 1100. Mass spectra were measured with an Agilent quadrupole 6110 spectrometer using an ESI+APCI source coupled to an Agilent 1200 HPLC system or an 1100 series LC/MSD trap spectrometer using an ESI source coupled to an Agilent 1100 HPLC system. The IC_{50} values were calculated using XL-Fit 2.0 software. Compound purity was determined by

HPLC , which confirmed the purity of ≥ 95% for all final biological testing compounds. HPLC method: Aglilent 1200 HPLC, Column: SB-C18 5u 150 x 4.6 mm; Mobile phase: H_2O (0.1% formic acid) and MeOH (0.1% formic acid); Gradient: 5% MeOH in 0-10 min, 95% MeOH in 10−13 min, 5% MeOH in 13-16 min; Flow rate: 1 mL/min; Detector: 254 nm.

Preparation of (*S*)-2-(1-(9*H*-purin-6-yl)pyrrolidin-2-yl)-5-chloro-3-phenylpyrrolo[2,1-*f*][1,2,4]triazin-4(3*H*)-one (6)

tert-butyl (*S*)-2-((2-carbamoyl-3-chloro-1*H*-pyrrol-1-yl)carbamoyl)pyrrolidine-1-carboxylate (**30a**) : To a solution of 1-amino-3-chloro-1*H*-pyrrole-2-carboxamide (700 mg, 4.40 mmol) and (*S*)-1-(*tert*-butoxycarbonyl)pyrrolidine-2-carboxylic acid (1040 mg, 4.84 mmol) in THF was added EDC·HCl (950 mg, 4.95 mmol). The reaction mixture was stirred at room temperature for 3.5 h, then was diluted with water and extracted with EtOAc. The combined organic layers were dried over anhydrous Na_2SO_4, and concentrated to yield the **30a** as a white solid, which was used for the next step without further purification (1.25 g, 80%). ^{1}H NMR (400 MHz, DMSO-d_6) δ 11.28 (s, 0.6H), 11.27 (s, 0.4H), 7.49 (s, 1H), 7.09 (s, 0.6H), 7.03 (s, 0.4H), 6.82 (d, J = 3.2 Hz, 0.4H), 6.71 (d, J = 2.8 Hz, 0.6H), 6.17 (d, J = 2.8 Hz, 0.6H), 6.14 (d, J = 3.2 Hz, 0.4H), 4.19 – 4.12 (m, 1H), 3.39−3.32 (m, 1H), 3.28−3.20 (m, 1H), 2.17−2.02 (m, 2H), 1.88−1.71 (m, 2H), 1.37 (s, 3H), 1.33 (s, 6H). MS (m/z): 256.9 $(M\text{-Boc+H})^+$.

tert-butyl (*S*)-2-(5-chloro-4-oxo-3,4-dihydropyrrolo[2,1-*f*][1,2,4]triazin-2-yl)pyrrolidine-1-carboxylate (**31a**) : To a solution of **30a** (1.25 g, 3.51 mmol) in EtOH (40 mL) was added a solution of KOH (1.00 g, 17.56 mmol) in water (40 mL). The reaction mixture was heated to 100 ºC for 2 days. After cooling to room temperature, the mixture was diluted with water and adjusted to pH4.5 with aq.HCl (1.0 N). The resulting precipitate was filtered off and dried to give **31a** as a white solid (850 mg, 72%).[28] ^{1}H NMR (400 MHz, DMSO-d_6) δ 7.54 (d, J = 2.8 Hz,

0.6H), 7.51 (d, *J* = 2.8 Hz, 0.4H), 6.54-6.51 (m, 1H), 4.49−4.46 (m, 0.4H), 4.43 - 4.39 (m, 0.6H), 3.54−3.44 (m, 1H), 3.33−3.26 (m, 1H), 2.26−2.10 (m, 1H), 1.99 – 1.71 (m, 3H), 1.34 (s, 3H), 1.13 (s, 6H). MS (m/z): 338.7 $(M+H)^+$.

tert-butyl (*S*)-2-(5-chloro-4-oxo-3-phenyl-3,4-dihydropyrrolo[2,1-*f*][1,2,4]triazin-2-yl)pyrrolidine-1-carboxylate (**32a**): A mixture of **31a** (850 mg, 2.51 mmol), phenylboronic acid (613 mg, 5.02 mmol), molecular sieves (4Å, 2 g), $Cu(OAc)_2$, (915 mg, 5.02 mmol), and pyridine (1.00 mL, 12.55 mmol) in dry DCM (30 mL) was stirred overnight at room temperature under dry air. The mixture was concentrated in *vacuo* and purified by flash chromatography, eluting with 0−100% gradient of MeOH in H_2O, to yield **32a** as a white solid (250 mg, 24%).[29] ^{1}H NMR (400 MHz, DMSO-d_6) δ 7.67 (d, *J* = 2.8 Hz, 0.6H), 7.65 (d, *J* = 2.8 Hz, 0.4H), 7.62−7.46 (m, 4H), 7.33 (d, *J* = 7.2 Hz, 0.4H), 7.25 (d, *J* = 7.6 Hz, 0.6H), 6.66 - 6.63 (m, 1H), 4.21−4.17 (m, 0.4H), 4.16−4.13 (m, 0.6H), 3.46−3.36 (m, 1H), 3.25−3.17 (m, 1H), 2.12−1.64 (m, 4H), 1.34 (s, 3H), 1.25 (s, 6H). MS (m/z): 414.7$(M+H)^+$.

(*S*)-2-(1-(9*H*-purin-6-yl)pyrrolidin-2-yl)-5-chloro-3-phenylpyrrolo[2,1-*f*][1,2,4]triazin-4(3*H*)-one (6): A mixture of **32a** (250 mg, 0.603 mmol) in a solution of HCl in MeOH (4 N, 25 mL) was stirred at room temperature for 2 h. The mixture was concentrated in *vacuo*. The residue (40 mg, 0.13 mmol) was dissolved in *n*-BuOH (3 mL), and then 6-chloro-9*H*-purine (22 mg, 0.14 mmol) and Et_3N (0.10 mL, 0.65 mmol) were added. The reaction mixture was refluxed for 2 h. The mixture was concentrated to remove *n*-BuOH. The resulting residue was purified by flash chromatography, eluted with 0−100% gradient of MeOH in H_2O, to yield the target compound **6** as a white solid (35 mg, 63%). Purity: 96.0%. MS (m/z): 432.7 $(M+H)^+$. ^{1}H NMR (400 MHz, DMSO-d_6) δ: 12.95 (s, 1H), 8.65−8.05 (m, 3H), 7.72−7.40 (m, 5H), 6.57−6.50 (m,

1H), 5.34−5.26 (m, 0.5H), 4.67−4.59 (m, 0.5H), 4.33−4.25 (m, 0.5H), 4.11−4.03 (m, 0.5H), 3.89−3.83 (m, 0.5H), 3.62−3.58 (m, 0.5H), 2.35−2.15 (m, 2H), 1.98−1.81 (m, 2H).

Compounds **7-9** were prepared by a procedure similar to that described for the synthesis of **6.**

(*S*)-4-(2-(5-chloro-4-oxo-3-phenyl-3,4-dihydropyrrolo[2,1-*f*][1,2,4]triazin-2-yl)pyrrolidin-1-yl)-7*H*-pyrrolo[2,3-*d*]pyrimidine-5-carbonitrile (7). Purity: 99.4%. MS (m/z): 456.8 $(M+H)^+$. ^{1}H NMR (400 MHz, DMSO-d_6) δ 12.84 (s, 1H), 8.29 (s, 1H), 8.26 (s, 1H), 7.78−7.71 (m, 1H), 7.68−7.43 (m, 5H), 6.55 (d, J = 3.0 Hz, 1H), 4.68−4.60 (m, 1H), 4.12−4.03 (m, 1H), 3.97−3.86 (m, 1H), 2.36−2.15 (m, 2H), 2.04−1.86 (m, 2H).

(*S*)-2-(1-(9*H*-purin-6-yl)pyrrolidin-2-yl)-5-fluoro-3-phenylpyrrolo[2,1-*f*][1,2,4]triazin-4(3*H*)-one (8) Purity: 100%. MS (m/z): 416.8 $(M+H)^+$. ^{1}H NMR (400 MHz, CD_3OD) 8.24 (s, 1H), 8.03 (s, 1H), 7.84−7.41 (m, 5H), 7.15−7.09 (m, 1H), 6.30−6.15 (m, 1H), 5.65−5.50 (m, 0.5H), 4.91−4.85 (m, 0.5H), 4.42−4.37 (m, 0.5H), 4.23−4.13 (m, 0.5H), 4.05−3.95 (m, 0.5H), 3.85−3.78 (m, 0.5H), 2.37−1.97 (m, 4H).

(*S*)-2-(1-(9*H*-purin-6-yl)pyrrolidin-2-yl)-3-phenylpyrrolo[2,1-*f*][1,2,4]triazin-4(3*H*)-one (9) Purity: 96.1%. MS (m/z): 398.7 $(M+H)^+$. ^{1}H NMR (400 MHz, DMSO-d_6) δ 12.94 (s, 1H), 8.28-8.01 (m, 2H), 7.79-7.32 (m, 6H), 6.97-6.75 (m, 1H), 6.55-6.36 (m, 1H), 5.43-5.25 (m, 0.5H), 4.73-4.60 (m, 0.5H), 4.40-4.25 (m, 0.5H), 4.14-4.01 (m, 0.5H), 3.94-3.81 (m, 0.5H), 3.72-3.60 (m, 0.5H), 2.31-2.10 (m, 2H), 2.01-1.91 (m, 1H), 1.90-1.77 (m, 1H).

Preparation of 5-chloro-2-((2*S*,4*S*)-4-fluoro-1-(9*H*-purin-6-yl)pyrrolidin-2-yl)-3-phenylpyrrolo[2,1-*f*][1,2,4]triazin-4(3*H*)-one (10)

tert-butyl (2*S*,4*S*)-2-(5-chloro-4-oxo-3,4-dihydropyrrolo[2,1-*f*][1,2,4]triazin-2-yl)-4-fluoropyrrolidine-1-carboxylate (**33**): To a solution of **31c** (prepared by a procedure similar to

that described for the synthesis of compound **31a** using (2*S*,4*R*)-1-(*tert*-butoxycarbonyl)-4-hydroxypyrrolidine-2-carboxylic acid as the material instead of (*S*)-1-(*tert*-butoxycarbonyl)pyrrolidine-2-carboxylic acid) (400 mg, 1.73 mmol) in DCM (50 mL) was added DAST (726 mg, 4.52 mmol) at 0 ^{0}C. The resulting mixture was stirred at 0 ^{0}C for 1 h, then allowed to be warmed up to room temperature and stirred for another 1 h. After the addition of aq. $NaHCO_3$ (10 mL), the mixture was extracted with DCM. The organic layers were washed with brine, dried over anhydrous Na_2SO_4 and concentrated to give compound **33**, which was used in the next step without further purification.[30] MS (m/z): 257.0 $(M\text{-Boc}+H)^+$.

Compounds **10** was prepared by a procedure similar to that described for the synthesis of compound **6** using compound **33** as the starting material instead of **31a**. Purity: 95.1%. MS (m/z): 451.1 $(M+H)^+$. ^{1}H NMR (400 MHz, DMSO-d_6) δ: 8.38-8.10 (m, 3H), 7.71−7.52 (m, 4H), 7.46 (s, 1H), 6.59−6.49 (m, 1H), 5.39−5.29 (m, 1H), 4.88−4.34 (m, 1H), 4.24−3.93 (m, 2H), 2.31−2.17 (m, 2H).

Compounds **11-12** were prepared by a procedure similar to that described for the synthesis of **6**.**(*S*)-2-(1-(9H-purin-6-yl)pyrrolidin-2-yl)-5-chloro-3-(3-fluorophenyl)pyrrolo[2,1-*f*][1,2,4]triazin-4(3*H*)-one (11)** Purity: 97.5%. MS (m/z): 450.8 $(M+H)^+$. ^{1}H NMR (400 MHz, DMSO-d_6) δ: 12.96 (s, 1H), 8.24−8.20 (m, 1H), 8.10 (s, 1H), 7.66−7.39 (m, 5H), 6.60−6.52 (m, 1H), 5.36−5.30 (m, 0.5H), 4.68−4.62 (m, 0.5H), 4.35−4.29 (m, 0.5H), 4.12−4.06 (m, 0.5H), 3.92−3.86 (m, 0.5H), 3.73−3.67 (m, 0.5H), 2.28−2.22 (m, 1H), 2.05−1.86 (m, 3H).

(*S*)-4-(2-(4-oxo-3-phenyl-3,4-dihydropyrrolo[2,1-*f*][1,2,4]triazin-2-yl)pyrrolidin-1-yl)-7*H*-pyrrolo[2,3-*d*]pyrimidine-5-carbonitrile (12) Purity: 97.0%. MS (m/z): 422.6 $(M+H)^+$. ^{1}H NMR (400 MHz, DMSO-d_6) δ: 12.81 (s, 1H), 8.27−8.26 (m, 2H), 7.72−7.68 (m, 1H), 7.64−7.41 (m, 5H), 6.88 (dd, J = 4.3, 1.7 Hz, 1H), 6.47 (dd, J = 4.3, 2.7 Hz, 1H), 4.72−4.65 (m, 1H),

4.12−4.06 (m, 1H), 3.96−3.89 (m, 1H), 2.35−2.15 (m, 2H), 2.06−1.83 (m, 2H). **4-((2*S*,4*S*)-2-(5-chloro-4-oxo-3-phenyl-3,4-dihydropyrrolo[2,1-*f*][1,2,4]triazin-2-yl)-4-fluoropyrrolidin-1-yl)-7*H*-pyrrolo[2,3-*d*]pyrimidine-5-carbonitrile (13).** Compound was prepared by a procedure similar to that described for the synthesis of compound **6** using compound **33** as the starting material instead of **31a**. Purity: 95.3 %. MS (m/z): 475.1 $(M+H)^+$. ^{1}H NMR (400 MHz, CD_3OD) δ: 8.23 (s, 1H), 7.98 (s, 1H), 7.75 (d, *J* = 8.0 Hz, 1H), 7.65−7.55 (m, 3H), 7.48 (d, *J* = 7.6 Hz, 1H), 7.30 (d, *J* = 3.0 Hz, 1H), 6.46 (d, *J* = 3.0 Hz, 1H), 5.39−5.31 (m, 1H), 5.22−5.16 (m, 1H), 4.56−4.41 (m, 2H), 2.51−2.41 (m, 1H), 2.22−2.16 (m, 1H).

(*S*)-2-(1-(5-acetyl-7*H*-pyrrolo[2,3-*d*]pyrimidin-4-yl)pyrrolidin-2-yl)-5-chloro-3-phenylpyrrolo[2,1-*f*][1,2,4]triazin-4(3*H*)-one (14). Compound was prepared by a procedure similar to that described for the synthesis of **6.** Purity: 98.9%. MS (m/z): 474.1 $(M+H)^+$. ^{1}H NMR (400 MHz, DMSO-d_6) δ: 12.29 (br, 1H), 8.16 (s, 1H), 8.03 (s, 1H), 7.80−7.35 (m, 6H), 6.57 (s, 1H), 4.47−4.44 (m, 1H), 3.81−3.64 (m, 2H), 2.48 (s, 3H), 2.11−1.93 (m, 3H), 1.65−1.56 (m, 1H).

2-((2*S*,4*S*)-1-(5-acetyl-7*H*-pyrrolo[2,3-*d*]pyrimidin-4-yl)-4-fluoropyrrolidin-2-yl)-5-chloro-3-phenylpyrrolo[2,1-*f*][1,2,4]triazin-4(3*H*)-one (15). Compound was prepared by a procedure similar to that described for the synthesis of compound **6** using compound **33** as the starting material instead of **31a**. Purity: 97.0%. MS (m/z): 492.1 $(M+H)^+$. ^{1}H NMR (400 MHz, DMSO-d_6) δ: 12.42 (br, 1H), 8.23 (s, 1H), 8.13 (s, 1H), 7.64−7.55 (m, 1H), 7.54−7.45 (m, 5H), 6.59 (d, *J* = 3.0 Hz, 1H), 5.24−5.02 (m, 1H), 4.74−4.63 (m, 1H), 4.19−3.97 (m, 1H), 3.92−3.83 (m, 1H), 2.51 (s, 3H), 2.44-2.21 (m, 2H).

Compounds **16-24** were prepared by a procedure similar to that described for the synthesis of **6.**

(*S*)-2-(1-(5-acetyl-7*H*-pyrrolo[2,3-*d*]pyrimidin-4-yl)pyrrolidin-2-yl)-5-chloro-3-(3-fluorophenyl)pyrrolo[2,1-*f*][1,2,4]triazin-4(3*H*)-one (16) Purity: 98.3%. MS (m/z): 492.6 $(M+H)^+$. ^{1}H NMR (400 MHz, DMSO- d_6) δ: 12.28 (br, 1H), 8.17 (s, 1H), 8.04 (s, 1H), 7.66−7.31 (m, 5H), 6.58 (s, 1H), 4.59−4.38 (m, 1H), 3.94−3.62 (m, 2H), 2.48 (s, 3H), 2.15−1.89 (m, 3H), 1.67−1.64 (m, 1H).

(*S*)-2-(1-(5-acetyl-7*H*-pyrrolo[2,3-*d*]pyrimidin-4-yl)pyrrolidin-2-yl)-5-fluoro-3phenylpyrrolo[2,1-*f*][1,2,4]triazin-4(3*H*)-one (17) Purity: 98.1%. MS (m/z): 458.1 $(M+H)^+$. ^{1}H NMR (400 MHz, $CDCl_3$) δ 11.60 (s, 1H), 8.23 (s, 1H), 7.76 (d, J = 7.9 Hz, 1H), 7.64 (s, 1H), 7.62−7.46 (m, 3H), 7.30−7.26 (m, 1H), 7.08−7.00 (m, 1H), 6.16 (d, J = 3.1 Hz, 1H), 4.81 (t, J = 6.8 Hz, 1H), 4.04−3.92 (m, 1H), 3.88-3.72 (m, 1H), 2.59 (s, 3H), 2.18−2.09 (m, 1H), 2.08−1.93 (m, 3H).

(*S*)-2-amino-4-(2-(5-chloro-4-oxo-3-phenyl-3,4-dihydropyrrolo[2,1-*f*][1,2,4]triazin-2-yl)pyrrolidin-1-yl)pyrimidine-5-carbonitrile (18) Purity: 98.9%. MS (m/z): 433.1 $(M+H)^+$. ^{1}H NMR (400 MHz, DMSO-d_6) δ 8.18 (s, 1H), 7.85 (d, J = 7.7 Hz, 1H), 7.60−7.46 (m, 5H), 6.97 (br, 2H), 6.59 (d, J = 3.0 Hz, 1H), 4.57−4.56 (m, 1H), 3.93 (br, 1H), 3.77−3.73 (m, 1H), 2.07−2.04 (m, 2H), 1.89 (br, 1H), 1.70−1.60 (m, 1H).

(*S*)-2-(1-(9*H*-purin-6-yl)azetidin-2-yl)-5-chloro-3-phenylpyrrolo[2,1-*f*][1,2,4]triazin-4(3*H*)-one (19) Purity: 97.4%. MS (m/z): 418.7 $(M+H)^+$. ^{1}H NMR (400 MHz, DMSO-d_6) δ: 12.93 (s, 1H), 8.18 (s, 1H), 8.09 (s, 1H), 7.72−7.41 (m, 6H), 6.59 (s, 1H), 5.18−5.04 (m, 1H), 4.19−4.03 (m, 2H), 2.68−2.60 (m, 1H), 2.24−2.16 (m, 1H).

(*S*)-4-(2-(5-chloro-4-oxo-3-phenyl-3,4-dihydropyrrolo[2,1-*f*][1,2,4]triazin-2-yl)azetidin-1-yl)-7*H*-pyrrolo[2,3-*d*]pyrimidine-5-carbonitrile (20) Purity: 96.3%. MS (m/z): 442.8 $(M+H)^+$. ^{1}H NMR (400 MHz, DMSO-d_6) δ: 8.24−8.23 (m, 2H), 7.70−7.41 (m, 6H), 6.61 (s, 1H),

5.13−5.05 (m, 1H), 4.38−4.28 (m, 1H), 4.15−4.09 (m, 1H), 2.66−2.58 (m, 1H), 2.10−1.98 (m, 1H).

(*S*)-2-(1-(5-acetyl-7H-pyrrolo[2,3-*d*]pyrimidin-4-yl)azetidin-2-yl)-5-chloro-3-phenylpyrrolo[2,1-*f*][1,2,4]triazin-4(3*H*)-one (21). Purity: 96.3%. MS (m/z): 460.2 $(M+H)^+$. ^1H NMR (400 MHz, DMSO-d_6) δ: 12.41 (s, 1H), 8.21 (s, 1H), 8.14 (s, 1H), 7.67−7.52 (m, 5H), 7.49−7.43 (m, 1H), 6.66−6.62 (m, 1H), 5.05−4.95 (br, 1H), 4.33−4.23 (m, 1H), 3.78−3.72 (m, 1H), 2.49−2.44 (m, 1H), 2.40 (s, 3H), 1.89−1.79 (m, 1H).

(*S*)-2-amino-4-(2-(5-chloro-4-oxo-3-phenyl-3,4-dihydropyrrolo[2,1-*f*][1,2,4]triazin-2-yl)azetidin-1-yl)pyrimidine-5-carbonitrile (22) Purity: 98.4%. MS (m/z): 419.1 $(M+H)^+$. ^1H NMR (400 MHz, DMSO-d_6) δ 8.15 (s, 1H), 7.74 (s, 1H), 7.58−7.52 (m, 4H), 7.45−7.38 (m, 1H), 7.14 (br, 2H), 6.66 (d, J = 3.0 Hz, 1H), 5.04−4.80 (m, 1H), 4.10−4.00 (m, 2H), 2.58−2.51 (m, 1H), 2.09−2.00 (m, 1H).

(*S*)-2-(1-(2-amino-5-chloropyrimidin-4-yl)azetidin-2-yl)-5-chloro-3-phenylpyrrolo[2,1-*f*][1,2,4]triazin-4(3*H*)-one (23) Purity: 100%. MS (m/z): 428.0 $(M+H)^+$. ^1H NMR (400 MHz, DMSO- d_6) δ 7.71 (d, J = 2.8 Hz, 1H), 7.70 (s, 1H), 7.62-7.49 (m, 4H), 7.39−7.37 (m, 1H), 6.64 (d, J = 3.0 Hz, 1H), 6.28 (s, 2H), 4.81−4.77 (m, 1H), 4.18−4.12 (m, 1H), 4.02−3.96 (m, 1H), 2.46−2.39 (m, 1H), 2.01−1.95 (m, 1H).

(*S*)-2-(1-(2-amino-5-ethynylpyrimidin-4-yl)azetidin-2-yl)-5-chloro-3-phenylpyrrolo[2,1-*f*][1,2,4]triazin-4(3*H*)-one (24) Purity: 98.5%. MS (m/z): 418.0 $(M+H)^+$. ^1H NMR (400 MHz, $CDCl_3$) δ 8.00 (s, 1H), 7.60-7.47 (m, 3H), 7.40 (d, J = 7.5 Hz, 1H), 7.30 (d, J = 2.9 Hz, 1H), 7.15−7.10 (m, 1H), 6.49 (d, J = 3.0 Hz, 1H), 5.13−5.03 (m, 1H), 4.85 (s, 2H), 4.39−4.34 (m, 1H), 4.16−4.07 (m, 1H), 3.14 (s, 1H), 2.38−2.18 (m, 2H).

Preparation of (*S*)-2-(1-(2-amino-5-(methylsulfonyl)pyrimidin-4-yl)azetidin-2-yl)-5-chloro-3-phenylpyrrolo[2,1-*f*][1,2,4]triazin-4(3*H*)-one (25)

To a mixture of **25a** [W = 4-(2-amino-5-bromo)pyrimidinyl, R_1=Cl, R_3=H, n=0] (prepared by a procedure similar to that described for the synthesis of compound **6**, 50 mg, 0.110 mmol) in toluene (10 mL), were added sodium methanesulfinate (27 mg, 0.260 mmol), $Pd_2(dba)_3$ (24 mg, 0.026 mmol), Xantphos (31 mg, 0.052 mmol) and K_3PO_4 (56 mg, 0.260 mmol). The reaction mixture was purged by N_2, and then stirred at 120 ℃ under microwave condition for 6 h. After cooling to room temperature, the mixture was concentrated and purified by flash chromatography to give **25** (5 mg, 10%) as a white solid. Purity: 98.3%. MS (m/z): 471.9 $(M+H)^+$. ^{1}H NMR (400 MHz, CD_3OD) δ 8.31 (s, 1H), 7.66−7.52 (m, 4H), 7.37 (d, *J* = 3.0 Hz, 1H), 7.34−7.28 (m, 1H), 6.52 (d, *J* = 2.9 Hz, 1H), 5.15−5.12 (m, 1H), 4.53−4.46 (m, 1H), 4.20−4.14 (m, 1H), 3.10 (s, 3H), 2.41−2.33 (m, 1H), 2.21−2.11 (m, 1H).

Preparation of (*S*)-2-(1-(5-acetyl-2-aminopyrimidin-4-yl)azetidin-2-yl)-5-chloro-3-phenylpyrrolo[2,1-*f*][1,2,4]triazin-4(3*H*)-one (26)

1-(2-amino-4-chloropyrimidin-5-yl)ethan-1-one ： To a solution of 1-(4-chloro-2-(methylthio)pyrimidin-5-yl)ethan-1-one (1 g, 5 mmol) in DCM (60 mL) was added *m*-CPBA (3.5 g, 20 mmol). The resulting mixture was stirred at room temperature for 12 h. Then cooled to -5℃, the reaction mixture, bubbled with NH_3, was stirred at -5^{o}C for 1h. Precipitate was formed and filtered out. The filtrate was concentrated, and purified by flash chromatography, eluting with 0−100% gradient of MeOH in H_2O, to give 1-(2-amino-4-chloropyrimidin-5-yl)ethan-1-one as a white solid (650 mg, 76%). MS (m/z): 171.9 $(M+H)^+$.

26 was prepared by a procedure similar to that described for the synthesis of compound **6** using 1-(2-amino-4-chloropyrimidin-5-yl)ethan-1-one as the material instead of 4-chloro-7*H*-

pyrrolo[2,3-*d*]pyrimidine-5-carbonitrile. Purity: 99.7%. MS (m/z): 436.0 $(M+H)^+$. ^{1}H NMR (400 MHz, DMSO-d_6) δ 8.42 (s, 1H), 7.71−7.47 (m, 5H), 7.39−7.36 (m, 1H), 6.82 (s, 2H), 6.62 (d, *J* = 3.0 Hz, 1H), 4.87−4.75 (m, 1H), 4.15−4.08 (m, 1H), 3.29−3.28 (m, 1H), 2.43−2.35 (m, 1H), 2.23 (s, 3H), 2.03-1.75 (m, 1H).

Preparation of (*S*)-2-(1-(2-amino-5-(cyclopropanecarbonyl)pyrimidin-4-yl)azetidin-2-yl)-5-chloro-3-phenylpyrrolo[2,1-*f*][1,2,4]triazin-4(3*H*)-one (27) and (*S*)-2-(1-(2-amino-5-(2,2,2-trifluoroacetyl)pyrimidin-4-yl)azetidin-2-yl)-5-chloro-3-phenylpyrrolo[2,1-*f*][1,2,4]triazin-4(3*H*)-one (28)

(*S*)-5-chloro-2-(1-(5-(cyclopropanecarbonyl)-2-(methylthio)pyrimidin-4-yl)azetidin-2-yl)-3-phenylpyrrolo[2,1-*f*][1,2,4]triazin-4(3H)-one (**36a**). This compound was prepared by a procedure similar to that described for the synthesis of compound **6.** Purity: 98.6%. MS (m/z): 493.1 $(M+1)^+$. ^{1}H NMR (400 MHz, CD_3OD) δ 8.50 (s, 1H), 7.68 – 7.61 (m, 1H), 7.60 – 7.53 (m, 2H), 7.50 (d, J = 7.8 Hz, 1H), 7.34 (br, 1H), 7.32 – 7.27 (m, 1H), 6.52 (d, J = 3.0 Hz, 1H), 5.24 (br, 1H), 4.25-4.19 (m, 1H), 4.15 – 3.98 (m, 1H), 2.48-2.39 (m, 4H), 2.28 – 2.06 (m, 2H), 0.97 (br, 2H), 0.64 (br, 1H), 0.30 (br, 1H).

To a solution of **36a** (86 mg, 0.174 mmol) in DCM (10 mL) was added *m*-CPBA (117 mg, 0.522 mmol, 77%) at 0 ^{0}C. The reaction mixture was allowed to room temperature and stirred at for 1 h, then NH_3 was purged for 3 min. The resulting mixture was stirred at room temperature for 3 h. After concentration, the mixture was purified by p-TLC to give compound **27** as a white solid (22 mg, 27%). Purity: 100%. MS (m/z): 462.2 $(M+1)^+$. ^{1}H NMR (400 MHz, CD_3OD) δ 8.43 (s, 1H), 7.67 – 7.59 (m, 1H), 7.59 – 7.50 (m, 3H), 7.35 (s, 1H), 7.31 – 7.23 (m, 1H), 6.51 (d, *J* = 3.0 Hz, 1H), 5.19 (br, 1H), 4.21-4.15 (m, 1H), 3.85 (br, 1H), 2.39 – 2.31 (m, 1H), 2.2-2.15 (m, 1H), 2.10 – 2.00 (m, 1H), 0.99 – 0.83 (m, 2H), 0.69 (br, 1H), 0.40 (br, 1H).

Compound **28** was prepared by a procedure similar to that described for the synthesis of compound **27**. Purity: 99.0%. MS (m/z): 489.8 $(M+1)^+$. ^{1}H NMR (400 MHz, CD_3OD) δ 8.46-8.36 (m, 1H), 7.66 – 7.20 (m, 6H), 6.50 (d, J = 2.4 Hz, 1H), 5.38 (br, 0.6H), 5.05 (br, 0.4H), 4.44 (br, 0.4H), 4.28 (br, 0.6H), 3.99 (br, 0.6H), 3.46 (br, 0.4H), 2.38 (br, 1H), 2.21 (br, 0.6H), 2.03 (br, 0.4H).

Kinase Assays: PI3K kinases including p110α/p85α (#PV4788) and p110γ (#PV4786) were purchased from Invitrogen, and p110β/p85α (#14-603) and p110δ/p85α (#14-604) were from Millipore. Primary screening data and IC_{50} values were measured using Transcreener™ KINASE Assay. The assay can be carried out according to the procedures suggested by the manufacturer. It is a universal, homogenous, high throughput screening technology using a far-red, competitive fluorescence polarization immunoassay based on the detection of ADP to monitor the activity of enzymes that catalyze group transfer reactions. The Transcreener™ KINASE Assay was designed as a simple two-part, endpoint assay. In the first step, the 25 μL of kinase reaction was performed by preparing a reaction mixture containing 5 μL inhibitor (2% DMSO final concentration), 10 μL kinase buffer (50 mM HEPES, 100 mM NaCl, 1 mM EGTA, 0.03% CHAPS, 3 mM $MgCl_2$, and freshly supplemented 1 mM DTT), and 10 μL 30 μM PIP2 / 10 μM ATP. The plate was sealed and incubated for 80 min at rt. Next, 25 μL ADP detection mix was added per well. The plate was sealed again and incubated for 60 min at r.t., and fluorescence polarization was measured by Tecan Infinite F500 Reader. The mP values were calibrated according to the instruction manual. Polarization values were converted to ADP concentration (ATP conversion) according to the standard curve. ADP concentrations in duplicate wells were averaged. The inhibition ratio (IR) was calculated as follows: IR%=100%-ADP concentration of test compounds/ADP concentration of 100% ATP conversion control) × 100%.

Cellular Assays: Cells (PC-3 for PI3Kβ; RAW264.7 for PI3Kγ; Ramos for PI3Kδ) were seeded into 96-well cell culture-grade plates at a density of 50,000 cells/90 μL/well for PI3Kβ, 30,000 cells/90μL/well for PI3Kγ, 60,000 cells/80 μL/well for PI3Kδ of RPMI-1640 (Life Technologies, #A10491-01) with 10% FBS (GIBCO,, #10099-141). And cells were incubated overnight for PI3Kβ and PI3Kγ, 3h for PI3Kδ at 5% CO_2 and 37 °C. Compounds were added to the cells, resulting in a final DMSO concentration of 0.5%, and incubated for some time (PI3Kα: 2 h; PI3Kβ: 60 min; PI3Kγ: 30 min; PI3Kδ: 60 min) at 5% CO_2 and 37 °C. For PI3Kα and PI3Kβ, the cells were fixed with 100 μL of 4% pre-warmed paraformaldehyde (2% in final) for 45 min at room temperature. Otherwise, cells were stimulated with 10 nM C5a (PI3Kγ, R&D Systems, 2150-C5-025) for 5 min or 1 μg/mL of anti-human IgM (PI3Kδ, Jackson ImmunoResearch, 709-006-073) for 15 min, followed by fixation with 100 μL of 4% pre-warmed paraformaldehyde (2% final) for 45 min at room temperature.

Acumen Assay: Cells were permeabilized and then blocked with 1% BSA in PBS for 2 h at rt. 40 μL/well of anti-phospho-Akt (Ser473) rabbit antibody (Cell Signal, #4060L) was added at 1:400 dilution, and incubated at 4 °C overnight. After washing, 40 μL/well of donkey anti-rabbit Alex488 antibody (Invitrogen, #A11034) was added at a 1:1,000 dilution and followed by 90-min incubation at r.t. in the dark. The plates were washed twice and 40 μL/well of 1.5 μM (final) Propidium Iodide solution (Sigma-Aldrich, #P4170) was added at 1:1,000 dilution. After incubation at r.t. for 30 min in the dark, the plates were loaded onto the Acumen Explorer and scanned with appropriate instrument settings. The threshold for p-Akt signal was set and the percentage of p-Akt signal (p-Akt%) in each well was exported. The inhibition ratio was calculated: IR% = (pAkt% of stimulation - pAkt% of test compound) / (pAkt% of stimulation - pAkt% of no stimulation) × 100%. The IR% rates in duplicate wells were averaged.

Basophil Activation Assay in HWB: The assay in HWB was performed using the FlowCast basophil activation test according to the manufacturer's instructions (Orpegen pharma, #10-0500). Whole blood was pre-treated with the compound for 30 min. Cells were stimulated with anti-IgE (Abcam, # ab31180) for PI3Kδ, fMLP (Sigma, # F3506) for PI3Kγ, or IL-3 (Peprotech, #AF-200-03) as a negative control. The ratio of $CD63^+$ positive cells in compound-treated blood as compared to the untreated control was used to determine the percent inhibition by compound treatment. Data were plotted using Prism software and IC_{50} values were determined. Data were analyzed via one-way ANOVA, followed by Dunnett's test.

B Cell Activation Assay in HWB in vitro: Whole blood was pre-treated with the compound for 60 min. The blood was stimulated with anti-IgM (Jackson ImmunoResearch, #709-006-073) at 37 °C overnight. After RBC depletion, cells were harvested and stained with APC-labeled anti-CD19 antibody (BD Biosciences, #555415) and FITC-labeled anti-CD69 antibody (BD Biosciences, #555530) for flow cytometry analysis. Activated B cells were gated based on B220 and CD86 expression. The ratio of $CD19^+CD69^+$ positive cells in compound-treated blood as compared to the untreated control was used to determine the percent inhibition by compound treatment. Data were plotted using Prism software and IC_{50} values were determined. Data were analyzed via one-way ANOVA, followed by Dunnett's test.

B Cell Activation Assay in RWB in vitro: The blood was stimulated with anti-IgD (AbD Serotec, # MCA190) at 37 °C overnight. After RBC depletion, cells were harvested and stained with PE anti-B220 antibody (eBioscience, #12-0460-82) and FITC anti-CD86 antibody (eBioscience, #11-0860-81) for flow cytometry analysis. Activated B cells were gated based on B220 and CD86 expression. The ratio of $B220^+CD86^+$ positive cells in compound-treated blood

as compared to the untreated control was used to determine the percent inhibition by compound treatment. Data were plotted using Prism software and IC_{50} values were determined. Data were analyzed via one-way ANOVA, followed by Dunnett's test.

B Cell Activation Assay in RWB *ex vivo*: Female Wistar rats were pretreated with test compounds or vehicle. Whole blood samples were collected at designated time points post-dose for all dose groups. The blood was stimulated with anti-IgD (AbD Serotec, # MCA190) at 37 °C overnight. After RBC depletion, cells were harvested and stained with anti-B220 antibody (eBioscience, #12-0460-82) and FITC anti-CD86 antibody (eBioscience, #11-0860-81) for flow cytometry analysis. Activated B cells were gated based on B220 and CD86 expression. Plasma concentrations of the compounds were analyzed.

Neutrophil Migration in Rat Air Pouch Model: The backs of the female Wistar rats were shaved and 20 mL of sterile air was injected subcutaneously on day 1. 10 mL of sterile air was again injected to maintain the pouch on day 3. On day 6, rats were orally dosed with compounds or vehicle prior to KC/GRO treatment. 0.5h later, rats were injected in dorsal pouches with 1 mL of recombinant rat KC/GRO (2 μg/rat, Peprotech, #400-10). The corresponding controls receive 1 mL of 0.5% CMC in PBS. The animals were sacrificed at 4h after KC/GRO injection, and the cells in the air pouches were harvested by injecting 5 mL of PBS containing EDTA. Total cells were counted by Cellometer Auto T4, and then stained with anti-RGraulocyte-PE antibody (eBioscience, #12-0570) for flow cytometry analysis. Neutrophils were gated based on Graulocyte expression. The results were reported as the number of neutrophils per cavity. Data were analyzed via one-way ANOVA, followed by Dunnett's test.

Type II Collagen Induced Arthritis in Rats [28]**:** Female Wistar rats were anesthetized with isoflurane. 200 μg of bovine type II collagen (Condrex, #20021) in Freund's incomplete adjuvant (Sigma-Aldrich, #F5506) was injected intradermally at the base of the tail on days 0 and 6. Test compound, YiSaiPu (Shanghai CP Guojian, Shanghai, China, Lot: 20120739) or vehicle was orally dosed from day 10 onwards. Hind paw volume was measured with plethysmometer daily, and the area under the paw volume-time curves were calculated. The data from day 10 to day 16 were analyzed with Repeated Measures One Way ANOVA analysis followed by LSD test.

Rat and human Liver Microsome Stability Screening Study: Human and rat liver microsomes were both supplied by CellzDirect, Life Technologies (DURHAM NC, US). Glucose-6-phosphate (G-6-P), glucose-6-phosphate dehydrogenase (G-6-PD) and β-Nicotinamide adenine dinucleotide phosphate (NADP) were supplied by Sigma-Aldrich (Missouri, USA). The incubations were conducted in duplicate. In general, incubation mixtures consisted of rat or human liver microsomes (0.5 mg/mL), test compound (1 μM), $MgCl_2$ (final 3 mM), EDTA (final 1 mM), and NADPH regenerating system (containing 5 mM G-6-P, 1U/mL G-6-PD, and 1 mM NADP, which was prepared in 50 mM potassium phosphate buffer at pH 7.4 and preincubated at 37 °C water-bath for 10 min and then cooled on ice until added into the reaction system) with a final volume of 125 μL. The stock solution of test compound was prepared with DMSO first and then diluted to designated concentration. The contents of organic solvents in the final incubation system were no more than 1% (for DMSO, the controlled margin was 0.1%). The incubation was commenced by putting the incubation system into 37 °C water bath open to the air and maintained for 0 and 30 min. The incubation was typically terminated by adding 125 μL cold acetonitrile containing internal standard. The terminated incubation mixtures were centrifuged at 3000 g for 10 min, and then 10 mL of supernatant was injected for analysis.

Pharmacokinetic Studies: We dosed male SD rats with **26** (body weight 200-232 g), and beagle dogs (body weight 6-10 kg, 3 males and 3 females); both groups were fasted before dosing. The IV group received a dose of 2.5 mg/ kg with a dosing volume of 2 mL/kg via tail vein for rats, while 1.0 mg/ kg with a dosing volume of 0.4 mL/kg was used for dogs. The PO group was orally administered at a dose of 10 mg/kg with a dosing volume of 10 mL/kg for rats, while 5 mg/kg with a dosing volume of 2 mL/kg was used for dogs. The dose was formulated in a clear solution of acidic 20% HP-beta-CD adjusted with 10 N HCl to a final pH2.5 for rats, while 20% HP-beta-CD dissolved and adjusted with 1 N HCl and then 1 N NaOH to a final pH4.3 for dogs was used. The blood samples were collected at 0, 2, 10, 30 min, and 1, 2, 4, 6, 8, 24 h for the rat IV group, at 0, 5, 15, 30 min, and 1, 2, 4, 6, 8, 24 h for the rat PO group, while at 0, 2, 5, 15, 30 min, and 1, 2, 4, 6, 8, 24 h for the dog IV group, at 0, 15, 30 min, and 1, 2, 4, 6, 8, 24 h for the dog PO group. Plasma was isolated and the concentrations of the compound in the plasma were determined with LC/MS/MS after protein precipitation with acetonitrile. Pharmacokinetic parameters were calculated based on the plasma concentration-time data using Thermo Kinetica®.ASSOCIATED CONTENT

Supporting Information.

SMILES (CSV).

Experimental procedures for molecular docking and electronic density model, electrostatic surfaces of some lower affinity specificity, the effect of C5 substitutions on the pyrrolotriazinone electrostatic surface, the docking pose of compound **26** in PI3Kγ, the x-ray crystal structure of compound **26**, ^{1}HNMR data of intermediate **32e** and compounds **27-28**. This material is available free of charge via the Internet at http://pubs.acs.org.

AUTHOR INFORMATION

Corresponding Author

*Phone: +86-21-20673088. E-mail: guangxiud@hmplglobal.com.

ABBREVIATIONS

HWB, human whole blood; RWB, rat whole blood; RLM, rat liver microsomal; HLM, human liver microsomal; PKPD, pharmacokinetic and pharmacodynamics; DMPK, drug metabolism and pharmacokinetic; SnAr, nucleophilic aromatic substitution.

REFERENCES

1. Foster, F. M.; Traer, C. J.; Abraham, S. M., Fry, M. J. The Phosphoinositide (PI) 3-kinase Family. *J. Cell Sci*. **2003**, *116*, 3037–3040.

2. Cantley, L. C. The Phosphoinositide 3-Kinase Pathway. *Science,* **2002**, *296*, 1655−1657.

3. Wymann, M. P.; Pirola, L. Structure and Function of Phosphoinositide 3-Kinases. *Biochim. Biophys. Acta, Mol. Cell. Bio. Lip.* **1998**, *1436*, 127−150.

4. Kong, D.; Yamori, T. Phosphatidylinositol 3-Kinase Inhibitors: Promising Drug Candidates for Cancer Therapy. *Cancer Sci*. **2008**, *99*, 1734-1740.

5. Maira, S. M.; Voliva, C.; Garcia-Echeverria, C. Class IA Phosphatidylinositol 3-Kinase: from Their Biologic Implication in Human Cancers to Drug Discovery. *Expert. Opin. Ther. Targets*. **2008**, *12*, 223-238.

6. Rommel, C.; Camps, M.; Ji, H. PI3Kδ and PI3Kγ: Partners in Crime in Inflammation in Rheumatoid Arthritis and beyond? *Nat. Rev. Immunol*. **2007**, *7*, 191-201.

7. Okkenhaug, K. Signaling by the Phosphoinositide 3-Kinase Family in Immune Cells. *Annu. Rev. Immunol.* **2013**. *31*, 675–704.

8. Sasaki, T.; Irie-Sasaki, J.; Jones, R. G.; Oliveira-dos-Santos, A. J.; Stanford, W. L.; Bolon, B.; Wakeham, A.; Itie, A.; Bouchard, D.; Kozieradzki, I.; Joza, N.; Mak, T. W.; Ohashi, P. S.; Suzuki, A.; Penninger, J. M. Function of PI3Kγ in Thymocyte Development, T Cell Activation, and Neutrophil Migration. *Science*, **2000**, *287*, 1040-1046.

9. Camps, M.; Rückle, T.; Ji, H.; Ardissone, V.; Rintelen, F.; Shaw, J.; Ferrandi, C.; Chabert, C.; Gillieron, C.; Françon, B.; Martin, T.; Gretener, D.; Perrin, D.; Leroy, D.; Vitte, P.; Hirsch, E.; Wymann, M.P.; Cirillo, R.; Schwarz, M. K. and Rommel, C. Blockade of PI3Kgamma Suppresses Joint Inflammation and Damage in Mouse Models of Rheumatoid Arthritis. *Nat Med.* **2005**, *11*, 936–943.

10. Hayer, S.; Pundt, N.; Peters, M. A.; Wunrau, C.; Kühnel, I.; Neugebauer, K.; Strietholt, S.; Zwerina, J.; Korb, A. and Penninger, J. PI3Kgamma Regulates Cartilage Damage in Chronic Inflammatory Arthritis. *FASEB J*. **2009**, *23*, 4288–4298.

11. Bartok, B.; Boyle D. L.; Liu, Y.; Ren, P.; Ball, S. T.; Bugbee, W. D.; Rommel, C.; Firestein, G. S. PI3 kinase δ is a Key Regulator of Synoviocyte Function in Rheumatoid Arthritis. *Am. J. Pathol.* **2012**, *180*, 1906–1916.

12. Somoza, J. R.; Koditek, D.; Villasenor, A. G.; Novikov, N.; Wong, M. H.; Liclican, A.; Xing, W.; Lagpacan, L.; Wang, R.; Schultz,B. E.; Papalia, G. A.; Samuel, D.; Lad, L.; McGrath, M. E. Structural, Biochemical, and Biophysical Characterization of Idelalisib Binding to Phosphoinositide 3-Kinase δ. *J. Biol. Chem*. **2015**, *290* , 8439−8446.

13. Burris, H. A. 3rd; Flinn, I. W.; Patel, M. R.; Fenske, T. S.; Deng. C.; Brander, D. M.; Gutierrez, M.; Essell, J. H.; Kuhn, J. G.; Miskin, H. P.; Sportelli, P.; Weiss, M. S.; Vakkalanka, S.; Savona, M. R.; O'Connor, O. A. Umbralisib, a Novel PI3Kδ and Casein Kinase-1ε Inhibitor, in Relapsed or Refractory Chronic Lymphocytic Leukaemia and Lymphoma: an Open-label, Phase 1, Dose-escalation, First-in-human Study. *The Lancet. Oncology*, **2018**, *19*, 486-496.

14. (a) Cushing, T. D.; Hao, X.; Shin, Y.; Andrews, K.; Brown, M.; Cardozo, M.; Chen, Y.; Duquette, J.; Fisher, B.; Felix Gonzalez-Lopez de Turiso, He, X.; Henne, K. R.; Hu, Y.; Hungate, R.; Johnson, M. G.; Kelly, R. C.; Lucas, B.; McCarter, J. D.; McGee, L. R.; Medina, J. C.; Miguel, T. S.; Mohn, D.; Pattaropong, V.; Pettus, L.H.; Reichelt, A.; Rzasa, R. M.; Seganish, J.; Tasker, A. S.; Wahl, R. C.; Wannberg, S.; Whittington, D. A. Whoriskey, J.; Yu, G.; Zalameda, L.; Zhang, D.; Metz, D. P. Discovery and *in vivo* Evaluation of (*S*)‑*N*−(1-(7-Fluoro-2-(pyridin-2-yl)quinolin-3-yl)ethyl)−9*H*−purin-6-amine (AMG-319) and Related PI3Kδ Inhibitors for Inflammation and Autoimmune Disease. *J. Med. Chem.* **2015**, *58*, 480 -511.; (b) Allen, R. A.; Brookings, D. C.; Powell, M. J.; Delgado, J.; Shuttleworth, L. K.; Merriman, M.; Fahy, I. J.; Tewari, R.; Silva, J. P.; Healy, L. J.; Davies, G. C. G.; Twomey, B.; Cutler, R. M.; Kotian, A.; Crosby, A.; McCluskey, G.; Watt, G. F.; Payne, A. Seletalisib: Characterization of a Novel, Potent, and Selective Inhibitor of PI3Kδ. *J. Pharmacol. Exp. Ther*, **2017**, *361*, 429-440.; (c) Xie, C.; He, Y.; Zhen, M.; Wang, Y.; Xu, Y.; Lou, L. Puquitinib, a Novel Orally Available PI3Kδ Inhibitor, Exhibits Potent Antitumor Efficacy Against Acute Myeloid Leukemia. *Cancer Sci*. **2017**, *108*, 1476-1484.; (d) Hoegenauer, K.; Soldermann, N.; Zécri, F.; Strang, R. S.; Graveleau, N.; Wolf, R. M.; Cooke, N. G.; Smith, A. B.; Hollingworth, G. J.; Blanz, J.; Gutmann, S.; Rummel, G.;

Littlewood-Evans, A.; Burkhart, C. Discovery of CDZ173 (Leniolisib), Representing a Structurally Novel Class of PI3K Delta-Selective Inhibitors. *Med. Chem. Lett.*, **2017**, *8*, 975–980.

15. Evans, C. A.; Liu, T.; Lescarbeau, A.; Nair, S. J.; Grenier, L.; Pradeilles, J. A.; Glenadel, Q.; Tibbitts, T.; Rowley, A. M.; DiNitto, J. P.; Brophy, E. E.; O'Hearn, E. L.; Ali, J. A.; Winkler, D. G.; Goldstein, S. I.; O'Hearn, P.; Martin, C. M.; Hoyt, J. G.; Soglia, J. R.; Cheung, C.; Pink, M. M.; Proctor, J. L.; Palombella, V. J.; Tremblay, M. R.; Castro, A. C. Discovery of a Selective Phosphoinositide-3-Kinase (PI3K)-γ Inhibitor (IPI-549) as an Immuno-Oncology Clinical Candidate. *Med. Chem. Lett*. **2016**, *7*, 862−867.

16. Rommel, C. Taking PI3Kδ and PI3Kγ One Step Ahead: Dual Active PI3Kd/g Inhibitors for the Treatment of Immune-Mediated Inflammatory Diseases. *Current Topics in Microbiology and immunology.* **2010**, *346*, 279-299.

17. Williams, O.; Houseman, B. T.; Kunkel, E. J.; Aizenstein, B.; Hoffman, R.; Knight, Z. A.; Shokat, K. M. Discovery of Dual Inhibitors of the Immune Cell PI3Ks p110δ and p110γ: A Prototype for New Anti-inflammatory Drugs. *Chem. Bio.* **2010**, *17*, 123-124.

18. Pillinger, G.; Loughran, N. V.; Piddock, R. E.; Shafat, M. S.; Zaitseva, L.;Abdul-Aziz, A.; Lawes, M. J.; Bowles, K. M.; Rushworth S. A. Targeting PI3Kδ and PI3Kγ Signalling Disrupts Human AML Survival and Bone Marrow Stromal Cell Mediated Protection. *Oncotarget*. **2016**; *7*, 39784-39795.

19. Piddock, R. E.; Loughran, N.; Marlein, C. R.; Robinson, S.D.; Edwards, D. R.; Yu, S.; Pillinger, G. E.; Zhou, Z.; Zaitseva, L.; Auger, M. J.; Rushworth, S. A.; Bowles, K. M.

PI3Kδ and PI3Kγ Isoforms Have Distinct Functions in Regulating Pro-tumoural Signalling in the Multiple Myeloma Microenvironment. *Blood Cancer Journal*, **2017**, *7*, e539;

20. Winkler, D. G.; Faia, K. L.; DiNitto, J. P.; Ali, J. A.; White, K. F.; Brophy, E. E.; Pink, M. M.; Proctor, J. L.; Lussier, J.; Martin, C. M.; Hoyt, J. G.; Tillotson, B.; Murphy, E. L.; Lim, A. R.; Thomas, B. D.; MacDougall, J. R.; Ren, P.; Liu, Y.; Li, L.; Jessen, K. A.; Fritz, C. C.; Dunbar, J. L.; Porter, J. R.; Rommel, C.; Palombella, J.; Changelian, P. S.; Kutok, J. L.; PI3K-δ and PI3K-γ Inhibition by IPI-145 Abrogates Immune Responses and Suppresses Activity in Autoimmune and Inflammatory Disease Models. *Chem. Bio*. **2013**, *20*, 1364-1374.

21. Leff, R**.;** Kumar, S.; Nikulenkova, N.; Kaidashev, I.; Allen, K.; Dunbar, J.; Stern, H.; Adams J.; Weinblatt, M. Safety and Efficacy Results of a Phase 2, Double-Blind, Placebo-Controlled Clinical Study of Duvelisib with Background Methotrexate (MTX) in Adults with Moderate-to-Severe Rheumatoid Arthritis (RA). **2015** ACR/ARHP Annual Meeting, San Francisco, abstract 2138.

22. Routhu, K.; Govindrajulu, B.; Veeraraghavan, S.; Viswanadha, S.; Vakkalanka S. RP6503, A Novel and Selective PI3K δ/γ Inhibitor, Potentiates the Effect of Steroids in Preclinical Models of COPD. *Eur. Respir. J*. **2014**, *44*, 1504.

23. Carlo-Stella, C.; Delarue, R.; Barde, P. J.; Scarfo, L.; Saheb, T.; Kumar, U.; Viswanadha, S.; Gandolfi, S.; Pittari, V.; Santoro, A.; Locatelli, S. L.; Vakkalanka, S.; Ghia, P.; Ferreri, A. J. M. A Dose Escalation Study of RP6530, a Novel Dual PI3K Delta/Gamma Inhibitor, in Patients with Relapsed/Refractory Hematologic Malignancies. **2015** American Society of Hematology, Orlando, abstract 623.

24. Knight, Z. A.; Gonzalez, B.; Feldman, M. E.; Zunder, E. R.; Goldenberg, D. D.; Williams, O.; Loewith, R.; Stokoe, D.; Balla, A.; Toth, B.; Balla, T.; Weiss, W. A.; Williams R. L.; Shokat, K. M. A Pharmacological Map of the PI3-K Family Defines a Role for p110a in Insulin Signaling. *Cell*, **2006**, *125*, 733–747.

25. Berndt, A.; Miller, S.; Williama, O.; Le, D. D.; Houseman, B. T.; Pacold, J. I.; Gorrec, F.; Hon, W.; Ren, P.; Liu, Y.; Rommel, C.; Gaillard, P.; Rückle, T.; Schwarz, M. K.; Shokat, K. M.; Shaw J. P.; Williams, R. L. The p110δ Structure: Mechanisms for Selectivity and Potency of New PI(3)K Inhibitors. *Nat. Chem. Bio,* **2010**, *6,* 117–124.

26. BROOD 3.1.0.3: OpenEye Scientific Software, Santa Fe, NM. http://www.eyesopen.com.

27. EON 2.3.0.3: OpenEye Scientific Software, Santa Fe, NM. http://www.eyesopen.com.Cope, A. P. Arthritis Research: Methods and Protocols. **2007**, *2*, 209.

28. Sampognaro, A. J.; Wittman, M. D.; Carboni, J. M.; Chang, C.; Greer, A. F.; Hurlburt, W. W. ; Sack, J. S.; Vyas, D. M. Proline Isosteres in a Series of 2,4-Disubstituted Pyrrolo[1,2-*f*][1,2,4]triazine Inhibitors of IGF-1R Kinase and IR Kinase. *Bio. Med. Chem. Lett.* **2010**, *20*, 5027-5030.

29. Ley, S. V.; Thomas, A. W. Modern Synthetic Methods for Copper-Mediated C(aryl)-O, C(aryl)-N, and C(aryl)-S Bond Formation. *Angew. Chem. Int. Ed.* **2003**, *42*, 5400-5449.

30. Bachand, C.; Belema, M.; Deon, D. H.; Good, A. C.; Goodrich, J.; James, C. A.; Lavoie, R.; Lopez, O. D.; Martel, A.; Meanwell, N. A.; Nguyen, V. N.; Romine, J. L.; Ruediger, E. H.; Snyder, L. B.; ST. Laurent, D. R.; Yang, F.; Langley, D. R.; Wang, G.; Hamann, L. G. Hepatitis C Virus Inhibitors. WO2008021927.

Table of Contents Graphic

A potent and highly selective PI3Kγ and PI3Kδ dual inhibitor was discovered from a selective PI3Kδ inhibitor.